Corrosion Science 164 (2020) 108340

Contents lists available at ScienceDirect

Corrosion Science

journal homepage: www.elsevier.com/locate/corsci

Enhanced corrosion protection by Al surface immobilization of in-situ grown layered double hydroxide films co-intercalated with inhibitors and low surface energy species

Yanhui Cao[a], Dajiang Zheng[b], Jingsong Luo[a], Fan Zhang[c], Cheng Wang[a], Shigang Dong[d], Yanlong Ma[e], Zhaoyuan Liang[e], Changjian Lin[a,*]

[a] College of Chemistry and Chemical Engineering, and State Key Laboratory for Physical Chemistry of Solid Surfaces, Xiamen University, Xiamen, Fujian 361005, P.R. China
[b] College of Materials, Xiamen University, Xiamen, Fujian 361005, P.R. China
[c] Division of Surface and Corrosion Science, Department of Chemistry, School of Chemical Science and Engineering, KTH Royal Institute of Technology, SE-100 44 Stockholm, Sweden
[d] College of Energy, Xiamen University, Xiamen, Fujian 361005, P.R. China
[e] College of Materials Science and Engineering, Chongqing University of Technology, Chongqing 400054, P.R. China

ARTICLE INFO

Keywords:
Aluminum
EIS
XRD
Interfaces
Neutral inhibition

ABSTRACT

In this work, a novel in-situ grown layered double hydroxide (LDH) film co-intercalated with inhibitors (vanadates) and low surface energy substance (laurates) was immobilized on Al substrates. A long-term monitoring of electrochemical impedance spectra (EIS) of the various samples in 3.5 wt.% NaCl solution demonstrated the synergetic protection of the intercalated two functional species. Meanwhile, the X-ray diffraction (XRD) result of the samples after immersion in NaCl solution for a long time presented the anion-exchange process between vanadates/laurates and chlorides. The synergetic effect of the two species loaded film significantly contributed to the enhanced long-term corrosion protection of aluminum.

1. Introduction

Corrosion of metals has resulted in not only tremendous loss of economy, but also serious waste of resources and occurrence of many disasters in all over the world. Therefore, corrosion control of metals is of valuable significance and facing long-term challenges. Researchers have developed various methods to protect metals from corrosion, such as organic coatings, inhibitors and cathodic protection, etc. In recent years, “smart” inhibitors have attracted much attention of researchers since they can provide corrosion protection only when corrosion is initiated. As reported in literature, polyelectrolyte nanocapsules, silica nanocapsules, polyurea microcapsules and chitosan polymers have been used as inhibitor-containing nano/micro-reserviors [1–6]. The loaded inhibitors can be released by trigger of pH, mechanical rupture and appearance of aggressive ions [7].

Layered double hydroxides (LDHs) can be used as inhibitor containers due to the large space in its gallery and the anion-exchange capacity [8]. The intercalated inhibitors can be released to the environment when aggressive anions such as chlorides appeared based on the anion-exchange reaction. In addition, LDHs possess a special property of the so-called memory effect. When LDHs are calcined at a moderate temperature, the layered structure would disappear and convert into metastable mixed oxides, and mixed oxides can recover the original layer structure when immersed in water or anionic solutions [9]. In recent years, LDHs have been widely used as “smart” containers in the field of corrosion protection of organic coatings and steel reinforced concrete [10–12]. It can be summarized that LDHs were used for corrosion protection in two different forms of powders and in-situ grown films on the surface of Al, Mg and their alloys.

In general, LDH powders can be synthesized by methods of co-precipitation, anion-exchange method and calcination-reconstruction. Among these methods, the last method was based on the above mentioned “memory effect” of LDHs. In our previous work, MgAl-LDH loaded with nitrites (MgAl-LDH-NO_2-) was synthesized by calcination reconstruction method and was added into concrete for corrosion protection. The long-term EIS results indicated this MgAl-LDH-NO_2^- was able to provide effective corrosion protection for carbon steel in concrete in a long time based on the mechanism of multifunctional

* Corresponding author.
E-mail address: cjlin@xmu.edu.cn (C. Lin).

https://doi.org/10.1016/j.corsci.2019.108340
Received 24 July 2019; Received in revised form 29 October 2019; Accepted 8 November 2019
Available online 12 November 2019
0010-938X/

corrosion protection. The multifunctional inhibitor contributed to the enhanced corrosion resistance by playing several different roles including absorbing chlorides, releasing nitrites and hydroxides [13]. In addition, Zuo et al. compared the properties of Mg-Al layered double hydroxides intercalated with nitrite ions prepared by calcined-rehydration, hydrothermal and co-precipitation method. The results indicated that the samples synthesized by co-precipitation method exhibited the largest capacity of chlorides and better anticorrosion effect [12]. Alibakhshi et al. carried out a comparative study on corrosion inhibitive effect of nitrate and phosphate intercalated ZnAl-LDH by incorporating them into a hybrid silane film covered by an epoxy topcoat. The presence of ZnAl-LDH-PO_4 endowed the coating with a strong self-healing ability when an artificial scratch was produced on it [14,15]. Mei et al. added aminobenzoate intercalated layered double hydroxides into epoxy coating on steel surface in simulated concrete pore solutions and it was found that proper dosage was able to increase obviously the corrosion resistance of the epoxy coating [16]. In addition to powders, LDH films can grow on the surface of Al, Mg and their alloys with high adhesion strength. In recent years, the in-situ grown LDH films were widely studied for corrosion protection for the underlying substrate. Duan's group fabricated NiAl-LDH films on Al substrate by a hydrothermal method successfully [17]. Many researchers focused their attention on the influence of preparation conditions on the morphology, composition and protective performance of the LDH films such as reactant concentration, reaction time and temperature. Tedim et al. reported that increase of Zn^{2+} concentration could lead to thicker films. However, the best performance was obtained for films synthesized at lower concentrations since no cracks appeared in this case [18]. The crystalline and compactness of LDHs increased with the increase of hydrothermal time and temperature [19,20]. It is worthy to note that Mikhailau et al. successfully fabricated ZnAl-LDH-NO_3 conversion coatings on zinc for the first time by one-step approach and a LDH growth model involving both electrochemical and chemical process was suggested [21]. In addition, the in-situ observation of the growth of ZnAl-LDH-NO_3 film was studied in detail by electrochemical quartz crystal microbalance (EQCM) and OCP recording [22]. As the as-prepared LDH films usually have many pore defects which allow water molecules and aggressive chlorides to reach the underlying substrate, researchers have developed different methods to address this problem. Zhang et al. sealed the micropores by depositing SiO_2 sol-gel, which gave excellent barrier property to the composite film as a result of its better compactness [23]. In addition, graphene layer was also prepared on LDH films by dip-coating method [24]. Yan et al. developed one-step in situ method to obtain reduced graphene/Zn-Al layered double hydroxide film with enhanced impermeability on magnesium alloys, which could effectively improve the corrosion resistance by preventing corrosion species from reaching the substrate [25]. Further modifications were also performed including loading inhibitors and low surface energy species. Tedim et al. intercalated vanadates into the gallery of ZnAl-LDH films and investigated its self-healing ability by scanning vibrating electrode technique (SVET) [26]. Wang and Anjum et al. synthesized MgAl-LDH on Al substrate and carried out chemical modification of the coating with 8-hydroxyquinolate anions (8-HQ). The EIS results indicated that the coating had superior self-healing protection ability [8,27]. Wu et al. prepared MgAl-LDH on Mg alloy using the anodic films as a source of cations without the introduction of any kinds of trivalent metal salts. The vanadate loaded LDHs presented better corrosion resistance compared to LDHs without vanadates [28]. Zhang et al. prepared a smart coating based on MgAl-layered double hydroxide on a cerium-modified plasma electrolytic oxidation coating on Mg AZ31 alloy. The results indicated that the synergistic effect between Ce species and the intercalated phosphate led to the superior corrosion protection effect [11]. Besides, various low surface energy species were used to obtain superhydrophobic surface of LDHs. Zhang et al. prepared laurates intercalated ZnAl-LDH on Al substrate and XRD results verified the successful intercalation of laurates into the gallery [29]. Their group also synthesized ternary ZnAlCu-LDH intercalated with laurates on Cu substrate [30]. The electrochemical test results indicated the anti-corrosion ability was improved due to an air film existing on the superhydrophobic surface. Wu et al. used different kinds of low surface energy species to modify MgAl-LDHs on magnesium alloy AZ31 [31]. The results demonstrated that the modification by fluoroalkylsilane could produce a better barrier to improve corrosion resistance of AZ31 Mg alloy than the fatty acid with long carbon chains due to the formation of the Si-O-surface bond by condensation polymerization reaction. In our previous work, we carried out a comprehensive characterization of the laurates intercalated ZnAl-LDH in terms of chemical stability, mechanical durability and long-term corrosion resistance in 3.5 wt.% NaCl solution to explore the potential application of ZnAl-LDH-La in industrial fields [32].

The above literature survey of LDHs demonstrates the advantageous performance of LDHs in corrosion protection. To the best of our knowledge, however, there has been no report of a LDH structure modified by two kinds of different species (inhibitors and low surface energy species). In this work, a novel ZnAl-LDH film loaded with both vanadates and laurates on Al substrate was fabricated. The laurate endows the LDH with superhydrophobicity and the vanadates act as inhibitor, both of which play a significant role in improving the corrosion resistance of LDH. Based on the long-term monitoring of EIS and XRD results, a synergetic corrosion protection mechanism was proposed.

2. Experimental

2.1. Materials and chemicals

Al (≥99.9 wt.%) plates (Huahuibo Platinum Nonferrous Metal Co. Ltd, Shenzhen, China) was cut into 2.3 cm × 2 cm × 0.3 cm. Zinc nitrate, sodium hydroxide, ammonium nitrate, and ethanol were purchased from Sinopharm Chemical Reagent Co. Ltd. 25 wt.% $NH_3{\cdot}H_2O$ and sodium chloride were purchased from Guangdong Guanghua Sci-Tech Co. Ltd., sodium vanadate and sodium laurate were purchased from Aladdin Industrial Corporation. All chemicals were used as received without further treatment. All the solutions were prepared with deionized water.

2.2. Synthesis of LDH films and further modification

In a typical procedure, the Al plates were abraded with emery sand paper of grade 400, 800, 1200 successively, and they were then cleaned in ethanol ultrasonically for 10 min and dried in ambient atmosphere naturally. The abraded Al plates were then etched in 0.1 M NaOH for 60 s to remove the oxide layer on the surface.

The surface treated Al substrates were vertically immersed in a mixed solution of 0.05 M $ZnNO_3$ and 0.3 M NH_4NO_3, the pH of which was adjusted to 6.5 by 1 wt.% $NH_3{\cdot}H_2O$. The hydrothermal reaction was performed in stainless hydrothermal reactor for 12 h at 85℃. When the reaction completed, the samples were washed by ethanol and dried in air naturally. The obtained samples were denoted as ZnAl-LDH-NO_3^-. ZnAl-LDH-NO_3^- were then immersed in 0.05 M aqueous sodium laurate solution for 4 h at 50℃. After washing by ethanol, the final product was labelled as ZnAl-LDH-La. Besides, ZnAl-LDH-NO_3- were immersed in 0.1 M $NaVO_3$ solution for 2 h at 50℃, the pH of which was adjusted to 8.4 with 0.1 M NaOH. The obtained samples were denoted as ZnAl-LDH-VOx. ZnAl-LDH-VOx was then immersed in 0.05 M aqueous sodium laurate solution for 4 h at 50℃. After washing, the final product was denoted as ZnAl-LDH-VOx-La.

2.3. Surface characterization

The top-view morphology of the surface of different samples was imaged by scanning electronic microscope (SEM, Hitachi FE-SEM

4800). The element composition was also analysed by energy dispersive X-ray spectroscopy (EDS). For cross-sectional view, the samples were machined by ultramicrotomy (UC; EM UC7, Leica, Germany) with a diamond knife. The cross-sectional images of the LDH films were obtained by field emission scanning electron microscopy (FE-SEM, JSM-7800 F, JEOL, Japan). The wide-angle X-ray diffraction (XRD) patterns were measured by the following conditions: 40 kV, 30 mA, and Cu Kα radiation (λ = 1.5406 Å), the samples were tested from 5 to 40° at a scanning rate of 10°/min. The small-angle XRD pattern was performed according to the following conditions: 35 kV, 15 mA, Cu Kα radiation (λ = 1.5406 Å), and the samples were tested from 2-10° at a scanning rate of 1°/min. Attenuated Total Reflection Fourier Transform Infrared spectroscopy (ATR-FTIR, Nicolet IS10 Thermo Scientific, USA) were obtained in the range of 4000–525 cm^{-1} at a resolution of 4 cm^{-1} using 16 scans, and diamond was used as the crystal. The static water contact angle (CA) and sliding angle (SA) were measured by a water drop volume of 4 μL with a dosing rate of 1 μL/s using a contact-angle meter (DSA100, Dataphysics, Germany) at ambient temperature.

2.4. Electrochemical measurements

The electrochemical experiments were performed in a three-electrode cell, where the platinum sheet was used as the counter electrode, the saturated calomel electrode (SCE) was used as the reference electrode and the prepared sample was used as the working electrode. The samples were immersed in 3.5 wt.% NaCl solution for at least 1 h to reach a steady state before they were subjected to electrochemical impedance spectra (EIS) test and the polarization test successively. The EIS test was carried out at OCP and the selected frequency range was from 100 kHz to 10 mHz with an amplitude of 10 mV. The EIS data were fitted using different equivalent circuits with Zview 3.1. The polarization curves were recorded from −0.2 V vs. OCP (SCE) to 0.2 V vs. OCP (SCE) at 1 mV/s. The related parameters including Tafel constants (b_a and b_c) and corrosion current densities (i_{corr}) were obtained by fitting the polarization data in the vicinity of E_{corr} ± 100 mV (SCE) by General Purpose Electrochemical System (GPES) equipped with Corrosion Rate Procedure carried out on an Autolab measurement system, which was adopted in the previous published work [14,30]. Each test was performed at least three times to guarantee the reproducibility. All the potentials in this paper were referred to SCE.

The EN measurements were carried out in a three electrode cell under OCP consisting of two identical electrodes with an artificial defect (dimension of 1 cm^2) and a saturated calomel reference electrode. Autolab ((Metrohm China Limited) was used for EN measurements with sampling of 2 Hz. The duration of the measurement was 1024s and the data was collected after immersion for 1 h, 4 h, 8 h and 24 h. The data were processed through Hilbert-Huang transform (HHT) using Matlab from MathWorks.

3. Results and discussion

3.1. Characterization

3.1.1. Morphologies and surface wettability of different LDH samples

The morphology of the as-prepared films was characterized by SEM images. As can be seen from Fig. 1a1 and a2, the ZnAl-LDH-NO_3^- was composed of curved hexagonal platelets lying perpendicularly to the substrate, which was in good accordance with the reported literature [33]. After treatment with sodium laurate, the morphology of the film changed considerably (Fig. 1b1 and b2). The LDH platelets were transformed from being perpendicular to the surface to disordered arrangement on the surface of Al substrate. It was reported that the disordered arrangement of LDH platelets may play a role in relieving the considerable stress induced by the intercalation of the laurate anions [29,30]. It can be clearly seen from Fig. 1c1 and c2 that the morphology almost remained unchanged after the intercalation with vanadates, except for that the thickness of the LDH platelets slightly increased. In Fig. 1d1 and d2, the LDH platelets also appeared randomly on the surface after modification with both sodium vanadate and sodium laurate, and related reasons have been demonstrated as above. Fig. 1a3-d3 presents the surface wettability of different samples. The ZnAl-LDH-NO_3- and ZnAl-LDH-VOx samples are hydrophilic with the water contact angles of 25.1 ± 0.3° and 19.7 ± 4.9°, respectively, while the samples of ZnAl-LDH-La and ZnAl-LDH-VOx-La are superhydrophobic with the water contact angles higher than 150°. In addition, the sliding angles of the two superhydrophobic samples were also measured, both of which were less than 3°. The side view of the above samples are shown in Fig. 2. The thickness of the ZnAl-LDH and ZnAl-LDH-VOx film was approximately 2.5 μm. After the intercalation of laurate anions in the gallery, the thickness of the ZnAl-LDH-La and ZnAl-LDH-VOx-La film increased obviously with an approximate value of 4.0 μm mainly induced by the intercalation of the laurate anions as the arbitrary arrangement of LDH platelets may play a role in relieving the considerable stress [29,30].

3.1.2. XRD spectra of different LDH samples

As can be seen from curve a in Fig. 3a, the XRD pattern of the ZnAl-LDH-NO_3^- film shows peaks at 9.9° and 19.9°, corresponding to the (003) and (006) reflections of an LDH phase with a basal spacing of 0.893 nm. This value was consistent with the reported literature for nitrate loaded ZnAl-LDH [34]. After immersion in 3.5 wt.% NaCl for 2 h, the peak attributed to (003) plane was split into two peaks (curve a in Fig. 3d). One still appeared at 10.0°, and the other appeared at 11.4°. The former peak can be assigned to the remaining nitrates in the gallery, while the latter one was due to newly intercalated chlorides as a result of the anion-exchange reaction between the nitrates in the gallery and the chlorides in the corrosive medium. This result verified the occurrence of the anion-exchange reaction. After treatment with sodium laurate, several peaks at low angles were observed (2.6°, 5.2°, 7.8°, 10.4°and 13.0°), which can be indexed as the (003), (006), (009), (0012) and (0015) reflections of a LDH phase (Fig. 3a curve b and Fig. 3b) [29,30]. According to the Bragg's Law, the gallery height can be calculated to be 3.40 nm, which was in good accordance with the value of laurate intercalated LDH in the reported literature [29,30]. After immersion in 3.5 wt.% NaCl solution for 2 h, the XRD pattern showed no obvious change compared with the as-prepared sample (Fig. 3d curve b and Fig. 3e). This was mainly due to an air film formed on the superhydrophobic surface, which impeded the contact between the LDH surface and the corrosive medium. After the ZnAl-LDH-NO_3- was modified by vanadates, the peaks corresponding to (003) and (006) reflections were shifted to the lower angles (Fig. 3a curve c), which appeared at about 9.3° and 18.8° with a basal spacing of 0.95 nm [35]. This verified the intercalation of $V_2O_7^{4-}$ via anion-exchange between nitrate in the interlayer and $V_2O_7^{4-}$ in the treatment solution. The curve c in Fig. 3d shows no change in comparison with curve c in Fig. 3a, indicating that chlorides failed to intercalate into the gallery of the LDH structure due to the strong affinity of $V_2O_7^{4-}$ with the interlayer [35]. As can be seen from Fig. 3a curve d and Fig. 3c, when the ZnAl-LDH-NO_3- was treated with sodium vanadate and sodium laurate successively, the obtained ZnAl-LDH-VOx-La presented peaks assigned to the intercalated $V_2O_7^{4-}$ (9.3°) and laurate (2.6°, 5.1°, 7.7°,10.4°and 12.9°), however, the intensity of the peaks decreased obviously, which may be caused by the co-intercalation of the two anions. After immersion in NaCl solution for 2 h, the peaks remained unchanged since chlorides didn't take part in anion-exchange reaction with vanadates and laurates.

3.1.3. Chemical composition of different samples after immersion in 3.5 wt.% NaCl solution

The EDS results were obtained from samples after immersion in 3.5 wt.% NaCl solution for 2 h. As can be seen from Fig. 4, Cl appeared only in the EDS spectrum of ZnAl-LDH-NO_3- with an atomic percentage

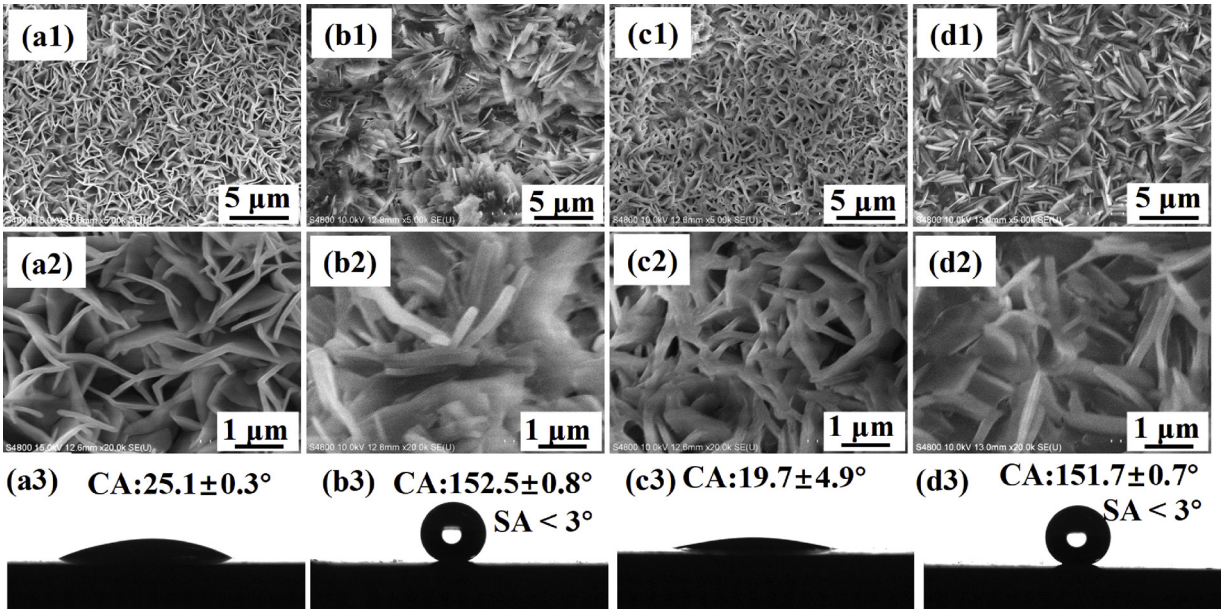

Fig. 1. Top-view and surface wettability of the as-prepared (a1, a2) ZnAl-LDH-NO_3-, (b1, b2) ZnAl-LDH-La, (c1, c2) ZnAl-LDH-VOx and (d1, d2) ZnAl-LDH-VOx-La at low and high magnification, respectively.

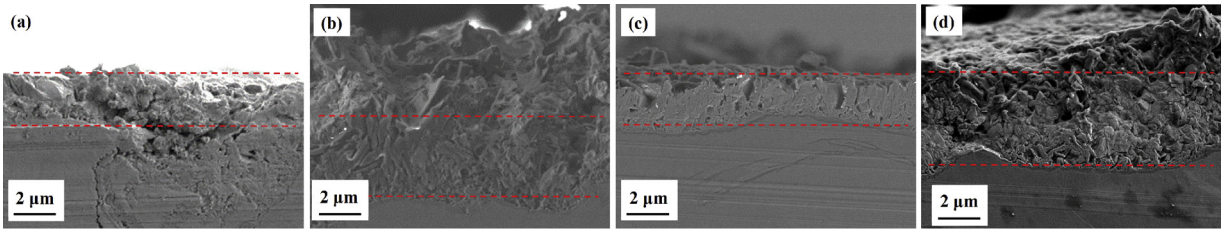

Fig. 2. Side-view of the as-prepared (a) ZnAl-LDH-NO_3^-, (b) ZnAl-LDH-La, (c) ZnAl-LDH-VOx and (d) ZnAl-LDH-VOx-La.

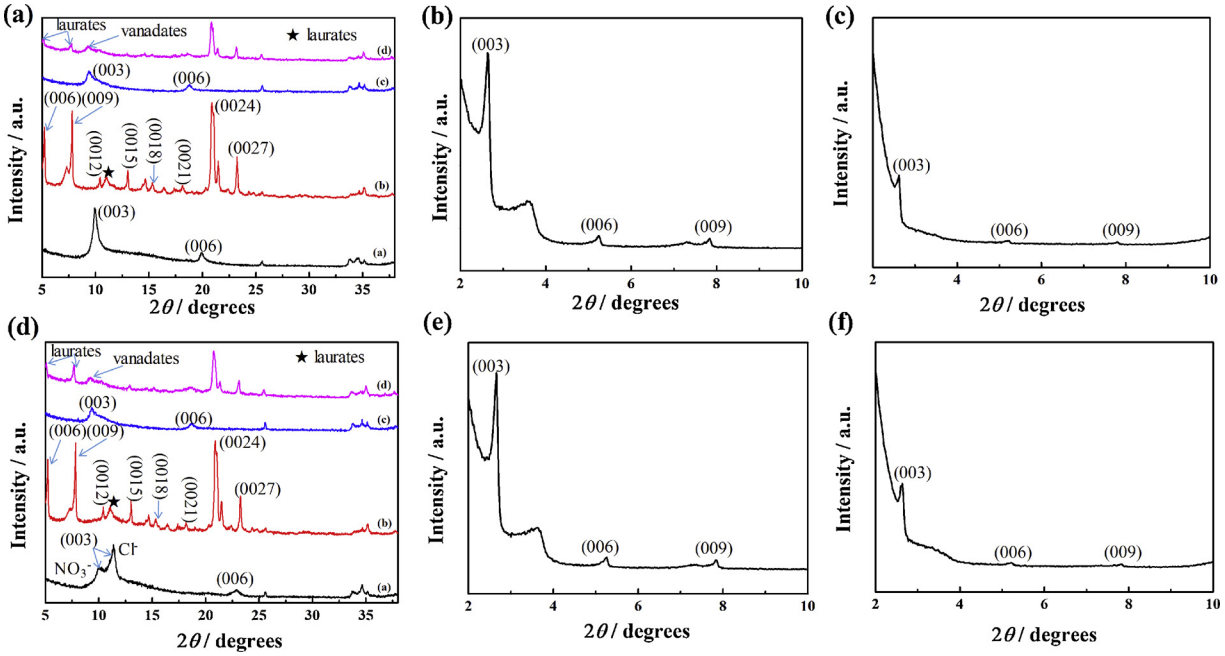

Fig. 3. Wide-angle XRD patterns of samples (a) as-prepared (d) after immersion in 3.5 wt.% NaCl solution for 2 h.(curve a: ZnAl-LDH-NO_3^-, curve b: ZnAl-LDH-La, curve c: ZnAl-LDH-VOx, curve d:ZnAl-LDH-VOx-La); small-angle XRD patterns of ZnAl-LDH-La (b) as-prepared and (e) after immersion in 3.5 wt.% NaCl solution for 2 h; small-angle XRD patterns of ZnAl-LDH-VOx-La (c) as-prepared and (f) after immersion in 3.5 wt.% NaCl solution for 2 h.

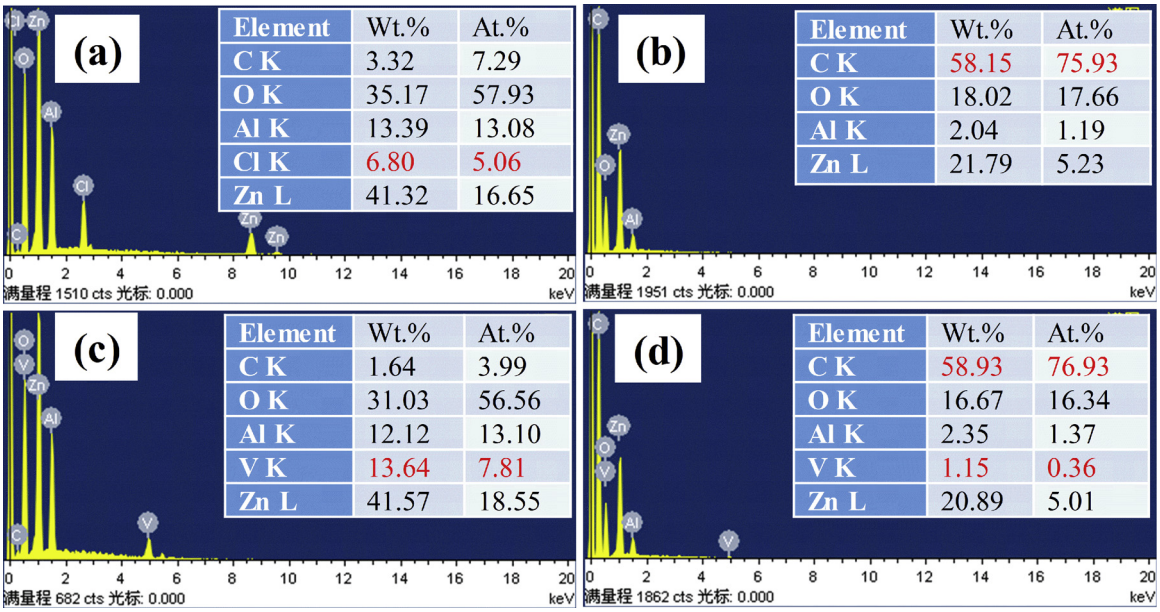

Fig. 4. EDS results of (a) the ZnAl-LDH-NO_3-, (b) ZnAl-LDH-La, (c) ZnAl-LDH-VOx and (d) ZnAl-LDH-VOx-La after immersion in 3.5 wt.% NaCl solution for 2 h.

about 5%. This is due to the anion-exchange reaction between the interlayer NO_3- with Cl- in the NaCl solution [36]. Nitrates are easier displaceable from the LDH structure compared with sulfate and carbonate anions. The reason for this phenomenon is that the propensity for some anions available in solution to exchange with "guest" anions in the LDH structure depends on the charge of anion involved [35]. Therefore, the nitrate intercalated LDHs are used as precursors for LDHs intercalated with other complex anions. As shown in Fig. 4b, Cl cannot be detected by EDS as a result of an air film formed on the superhydrophobic surface by the modification by laurates. The air film acted as a strong physical barrier, impeding the attack of water molecules and aggressive ions in the corrosive medium. Also, the C content increased dramatically, which can be attributed to the modification of laurates. In Fig. 4c, V appeared in the EDS spectra of ZnAl-LDH-VOx film, however, Cl was not observed since the anion-exchange reaction did not take place between the $V_2O_7^{4-}$ in the gallery and the chlorides in the solution during an immersion period of 2 h due to the strong affinity of the $V_2O_7^{4-}$ anions with the LDH layers. As can be seen from Fig. 4d, V appeared in the spectra and also C increased considerably, indicating the co-intercalation of vanadates and laurates. The sample containing vanadates and laurates shows a strong decrease in vanadates. The reasons can be stated as follows. On one hand, the co-intercalation of these two anions (vanadates and laurates) contributed to the less percentage of vanadates. On the other hand, lots of laurate anions adsorbed on the surface of LDH, which could also result in a decrease of detected vanadates [32]. The EDS results are in perfect accordance with the XRD results in Fig. 3.

3.1.4. ATR-FTIR result of different LDH samples

Fig. 5 depicts the ATR-FTIR spectra of different samples. The peaks at 1345 cm^{-1} and 1637 cm^{-1} in the spectrum of ZnAl-LDH-NO_3- can be attributed to the intercalated nitrate ions and the bending vibration of interlayer water molecules, respectively. A broad peak in the range of 3000 − 3500 cm^{-1} was due to the H−OH− stretching vibration of water molecules in the gallery of ZnAl-LDH-NO_3-. The peak occurred at 607 cm^{-1} belonged to Al-O vibration. In the spectra of ZnAl-LDH-La, two peaks appeared at 2918 cm^{-1} and 2849 cm^{-1}, which can be assigned to the alkyl C–H groups [37]. The other two peaks appearing at 1595 cm^{-1} and 1409 cm^{-1} were due to the asymmetric and symmetric vibration of COO- groups [38]. As for ZnAl-LDH-VOx, a small peak at 1356 cm^{-1} can be ascribed to the remaining nitrates in the gallery due to the

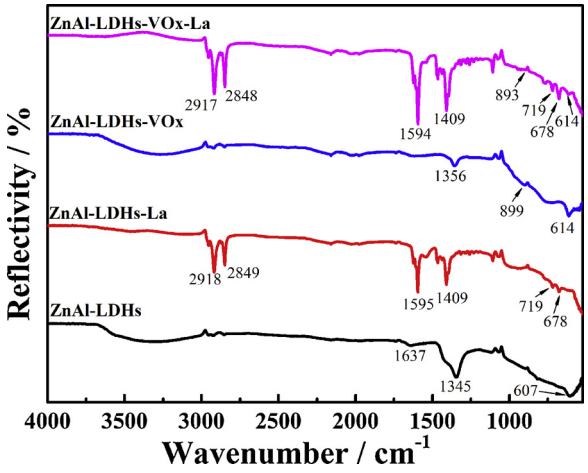

Fig. 5. ATR-FTIR spectra of as-prepared (a) ZnAl-LDH-NO_3-, (b) ZnAl-LDH-La, (c) ZnAl-LDH-VOx and (d) ZnAl-LDH-VOx-La.

incomplete anion-exchange reaction between nitrates and vanadates. In addition, a new peak occurred at 899 cm^{-1}, which was associated with the stretching vibration of vanadates, suggesting the presence of vanadates in the interlayer [28,39]. In the case of ZnAl-LDH-VOx-La, strong peaks at 2917 cm^{-1}, 2848 cm^{-1}, 1594 cm^{-1} and 1409 cm^{-1} were observed, indicating the existence of laurates in the gallery. Besides, a small peak belonging to vanadates at 893 cm^{-1} appeared. The above result demonstrates that the laurates and vanadates co-existed in ZnAl-LDHs-VOx-La.

3.2. The corrosion protection property of the prepared ZnAl-LDH films

3.2.1. Polarization test on different LDH samples

The protection behaviour of the LDH-related samples was evaluated by the polarization curves. Fig. 6 presents typical polarization curves of different samples in 3.5 wt.% NaCl solution. According to Fig. 6, bare Al substrate shows the highest corrosion current density among all the samples with a corrosion potential around -0.95 V (vs. SCE). When ZnAl-LDH-NO_3- film grew on the Al substrate, the corrosion potential was moved to the positive direction with a lower corrosion current density, indicating the protection effect of the ZnAl-LDH-NO_3- film for

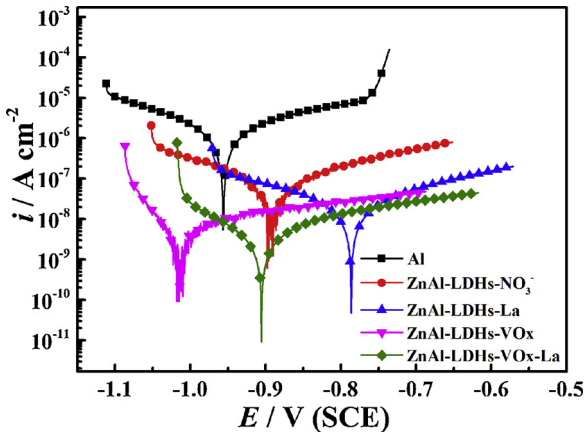

Fig. 6. Polarization curves in 3.5 wt.% NaCl solution of different samples.

Table 1
The electrochemical parameters estimated from polarization data in Fig. 6.

Samples	E_{corr}/mV (SCE)	b_a/mV dec^{-1}	b_c/mV dec^{-1}	i_{corr}/nA cm^{-2}
Al	−937 ± 19	644 ± 246	−336 ± 74	4454 ± 1360
ZnAl-LDH-NO_3-	−832 ± 11	756 ± 187	−422 ± 101	117.4 ± 35.0
ZnAl-LDH-La	−755 ± 32	323 ± 12	−359 ± 16	67.4 ± 22.5
ZnAl-LDH-VOx	−950 ± 65	200 ± 11	−67 ± 7	5.19 ± 0.068
ZnAl-LDH-VOx-La	−852 ± 54	252 ± 5	−165 ± 14	5.66 ± 0.056

the underlying substrate due to the physical barrier effect and the capacity of absorbing chlorides. When the ZnAl-LDH-NO_3- film was treated with sodium vanadate and sodium laurate, respectively, the obtained ZnAl-LDH-VOx and ZnAl-LDH-La shows further reduction of the corrosion current density, however, the corrosion potential of the former one was moved to the negative direction while the latter was moved to the positive direction obviously. It is worthy to note that the ZnAl-LDH-VOx-La demonstrates the lowest corrosion current density among all the samples, suggesting its effective protection effect for the underlying Al substrates. This can be attributed to the dual function of the intercalated vanadates and laurates. On one hand, the modification of laurates decreases the surface energy of ZnAl-LDH-VOx-La and makes it superhydrophobic, and the "air film" preventing the attack of water molecules and chlorides strongly. On the other hand, the intercalated vanadates closely interact with the LDHs layer and chlorides can hardly get into the gallery of LDHs by anion-exchange reaction with vanadates in the interlayer due to its strong affinity with LDHs in a short time. Also, vanadates can act as inhibitors and prevent the metal from corrosion.

The electrochemical parameters including the corrosion potential (E_{corr}), corrosion current density (i_{corr}) and the Tafel constants (β_c and β_a) were obtained by extrapolating the polarization data by General Purpose Electrochemical System (GPES) equipped with Corrosion Rate Procedure according to the following equation [40,41]:

$$i = i_{corr}\left\{\exp\left[\frac{2.303(E - E_{corr})}{b_a}\right] - \exp\left[\frac{2.303(E_{corr} - E)}{b_c}\right]\right\} \quad (1)$$

As can be seen from Table 1, the obtained corrosion current density shows the similar trend in Fig.6.

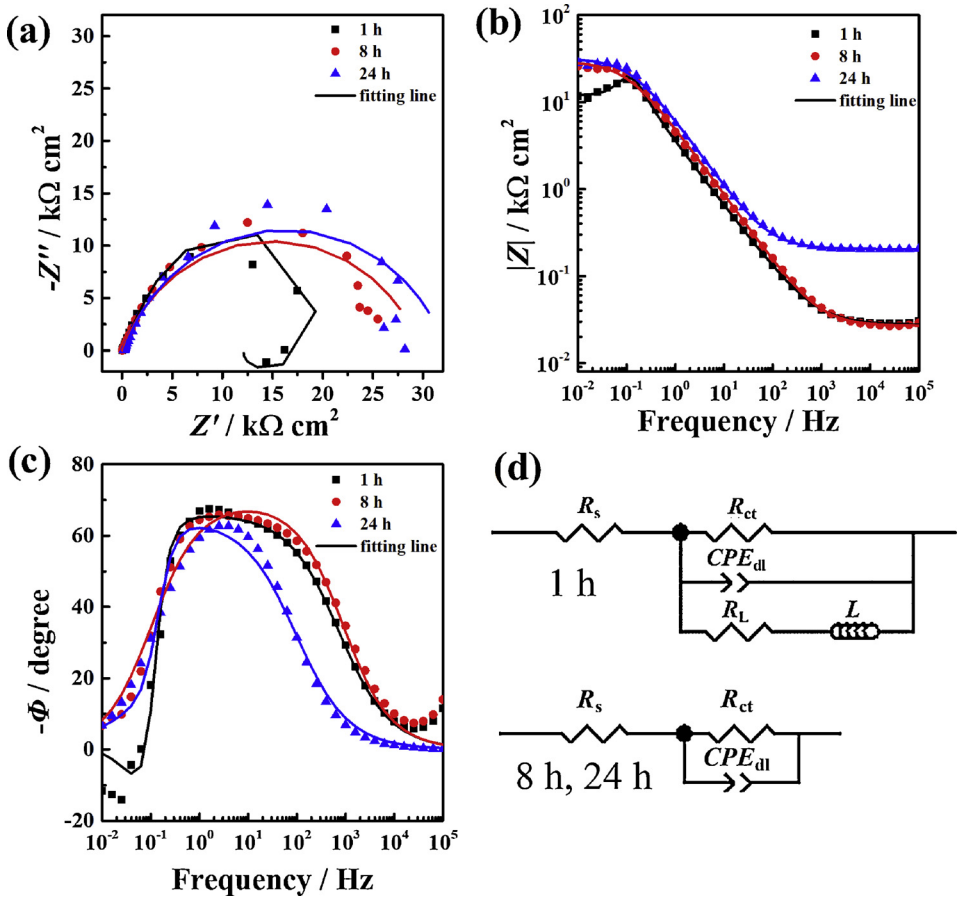

Fig. 7. (a) Nyquist plots, (b) Impedance-frequency Bode plots and (c) Phase-frequency Bode plots of blank Al in 3.5 wt.% NaCl solution after immersion for different time; (d) The equivalent circuit used to simulate EIS data at different stages.

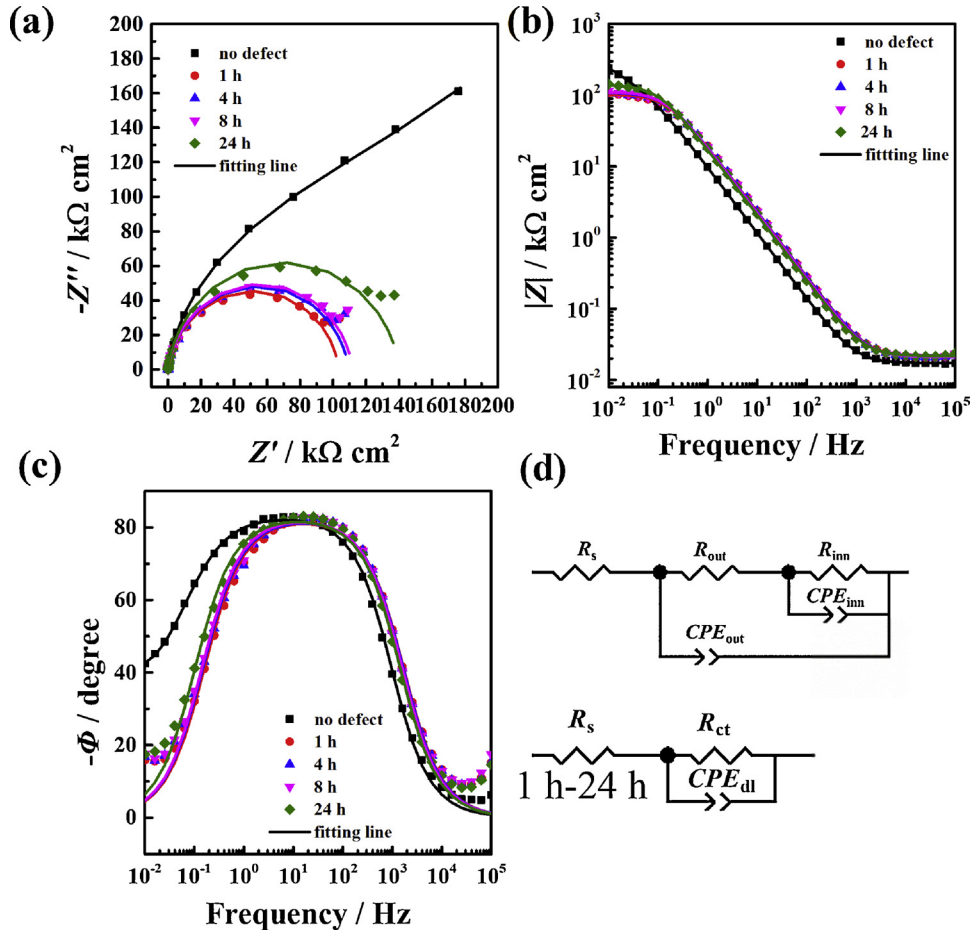

Fig. 8. (a) Nyquist plots, (b) Impedance-frequency Bode plots and (c) Phase-frequency Bode plots of ZnAl-LDH-NO_3- with an artificial defect in 3.5 wt.% NaCl solution after immersion for different time; (d) The equivalent circuit used to simulate EIS data at different stages.

3.2.2. EIS investigations of LDH samples with artificial defects

In order to investigate the self-healing ability of different LDH samples, a defect was made by a sharp knife on the surface of them and the underlying Al substrate was exposed. The artificial defect was 6 mm in length and 100 μm in width. The EIS tests were performed on different samples with an artificial defect immersed in 3.5 wt.% NaCl solutions for different exposure period. For comparison, blank Al substrate was subjected to the EIS test as well. Nyquist and Bode diagrams are presented in Figs. 7–11. In addition, the equivalent circuits used to fit the EIS data in different periods are also shown in each figure. The corresponding fitting results are shown in Tables 2–7.

Fig. 7 shows the EIS spectra changes of blank Al substrate along with the immersion time. It can be seen clearly that electrical inductance appeared in the Nyquist spectra in 1 h, indicating serious dissolution of Al. The electrical inductance disappeared after immersion for 8 h, which can be attributed to the accumulation of the corrosion products. The equivalent circuits in Fig. 7d were used for data fitting, where R_s represents the solution resistance, R_{ct} is the charge transfer resistance and *CPE* is the double layer capacitance. In addition, R_L is the inductance resistance and *L* means the electrical inductance. The fitting results of the EIS data based on the equivalent circuit are shown in Table 2.

In Fig. 8, the EIS spectra of ZnAl-LDH-NO_3- sample with an artificial scratch after immersion in NaCl for different time was demonstrated. For comparison, the sample without defect was also shown. It is clear that the impedance of ZnAl-LDH-NO_3- with defect declined greatly after immersion for 1 h in comparison with the sample without defect. This is because the underlying Al was exposed to the corrosive medium after the defect appeared and corrosion was initiated quickly. The impedance arc kept almost unchanged during the initial 8 h and increased obviously after 24 h. According to Fig. 8c, the phase angle peak narrowed after the defect appeared, which can be regarded as another signal of corrosion occurrence. Two equivalent circuits in Fig. 8d were chosen for fitting the EIS spectra of ZnAl-LDH-NO_3- without and with defect, respectively. In the first equivalent circuit, the R_s is the solution resistance, the first time constant is related to the outer porous LDH film response and the second time constant can be ascribed to the response of the inner compact LDH film [28]. R_{out} and R_{inn} are the resistance of the outer LDH film and the inner LDH film, respectively. In addition, CPE_{out} and CPE_{inn} are the constant phase element of the outer LDH film and the inner LDH film, respectively. There is one time constant in the second equivalent circuit, R_{ct} is the charge transfer resistance and CPE_{dl} is the double layer capacitance. They represent the response from the corrosion activities. The fitting results of the EIS data are shown in Table 3. According to Table 3, the values of R_{ct} remained almost stable in spite of some small fluctuations during the immersion of the first 8 h, and it increased considerably after 24 h, which were mainly due to the fact that more corrosion product accumulated at the corrosion sites and inhibited the development of corrosion to some degree.

As shown in Fig. 9, the impedance arc of ZnAl-LDH-La decreased dramatically upon the presence of the defect and it continued to decline gradually with time going on. The reasons can be explained as follows. The air film was destroyed and electrolyte reached the exposed substrates. The above result suggest that the intercalated laurates did not play a significant role in corrosion inhibition and corrosion propagated in this system. More detailed information can be obtained from the Bode plot in Fig. 9c. As can be seen from Fig. 9c, the intact ZnAl-LDH-La demonstrated an obvious phase angle peak at high frequencies, which

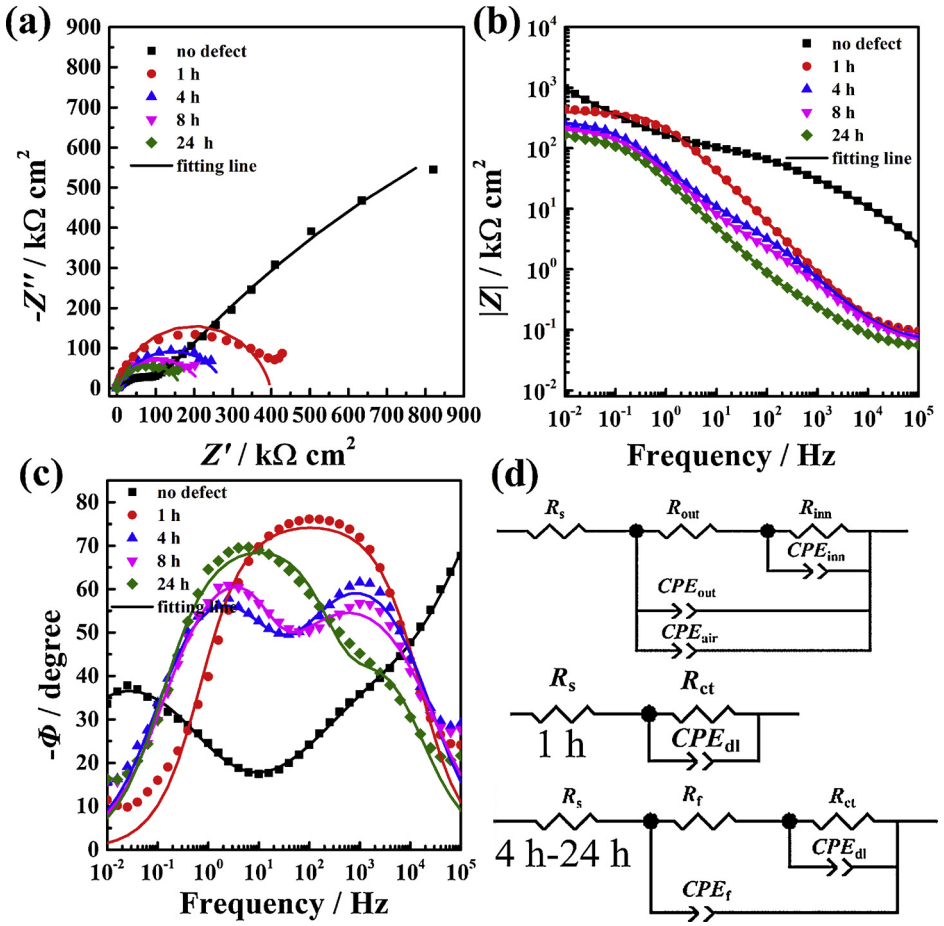

Fig. 9. (a) Nyquist plots, (b) Impedance-frequency Bode plots and (c) Phase-frequency Bode plots of ZnAl-LDH-La with an artificial defect in 3.5 wt.% NaCl solution after immersion for different time; (d) The equivalent circuit used to simulate EIS data at different stages.

can be ascribed to the insulative air film on the surface. The first equivalent circuit in Fig. 9d was used to fit the EIS data [32,42]. Among all the elements, CPE_{air} was introduced to describe the insulative air film in this system. In addition, R_{out} and CPE_{out} are the resistance and the constant phase element of the outer LDH film. In addition, R_{inn} and CPE_{inn} are the resistance and the constant phase element of the inner LDH film. However, only one phase angle peak can be observed after the defect was made for 1 h, corresponding to the occurrence of corrosion. The second equivalent circuit in Fig. 9d with one time constant related to the response of the corrosion reaction was used to fit the EIS data at this time. After immersion of 4 h, one additional phase angle peak occurred in the Bode spectra. According to the literature, the laurates are able to adsorb on the metal oxide surface by electrostatic interaction [37,43]. Therefore, the new phase angle peak can be attributed to the adsorption of laurates on the exposed surface at the defect area. However, it is reported that the interaction between the $-COO^-$ groups of aliphatic acid such as laurates and the surface are not strong enough due to the low electron density on $COO-^-$ and permeated aggressive chlorides can displace the adsorbed laurates gradually [43]. Consequentially, the new peak at high frequencies became obscure after immersion for 24 h in Fig. 9c. The third equivalent circuit in Fig. 9d with another additional time constant corresponding to the newly formed laurate film was adopted to simulate the EIS data in the immersion period of 4 h–24 h, where R_f and CPE_f represent the resistance and constant phase element of protective films formed from laurates. The fitting results are shown in Table 4. As can be seen from Table 4, the values of R_{ct} declined gradually, suggesting the propagation of corrosion. The higher R_{ct} values suggest a better protection ability of ZnAl-LDH-La in comparison with those of ZnAl-LDH-NO_3-. It can be concluded that the laurates play a role in preventing the attack of aggressive anions, however, the effect is not so conspicuous due to their own structure characteristics.

Fig. 10 presents the EIS spectra changes of ZnAl-LDH-VOx before and after the defect appeared. It is clear that the impedance arc declined considerably upon the presence of defect, demonstrating the initiation of corrosion. However, the impedance arc increased gradually with time going on, which can be attributed to the self-healing behaviour of the LDH film intercalated with vanadates. Once corrosion occurred, the loaded vanadates were released to the environment and acted as effective inhibitors. As a result, the defect sites were repaired and corrosion was inhibited efficiently. Accordingly, Fig. 10c presents the Bode plots at different immersion period. As can be seen from Fig. 10c, one additional phase angle peak can be observed for ZnAl-LDH-VOx upon the existence of defect, which probably corresponded to the compact film at the defect by the interaction between vanadates and surface. However, this newly peak became obscure after immersion of 24 h. The related reason was quite different from that for Fig. 9c. It was likely due to formation of a denser and more compact reparation film at the scratched area and the two phase angle peaks overlapped with each other because the resistance increased gradually [26,44–46]. The first equivalent circuit in Fig. 10d was adopted to simulate the data of ZnAl-LDH-VOx without defect. The meaning of all the element in this equivalent circuit was the same as those of ZnAl-LDH-NO_3- without defect. Another equivalent circuit consisting of two time constants was used for fitting ZnAl-LDH-VOx with a defect, where one time constant was related to the corrosion process and the other was associated with the reparation film formed at the defect area. R_{ct} is the charge transfer resistance and CPE_{dl} is the double layer capacitance. In addition, R_f and

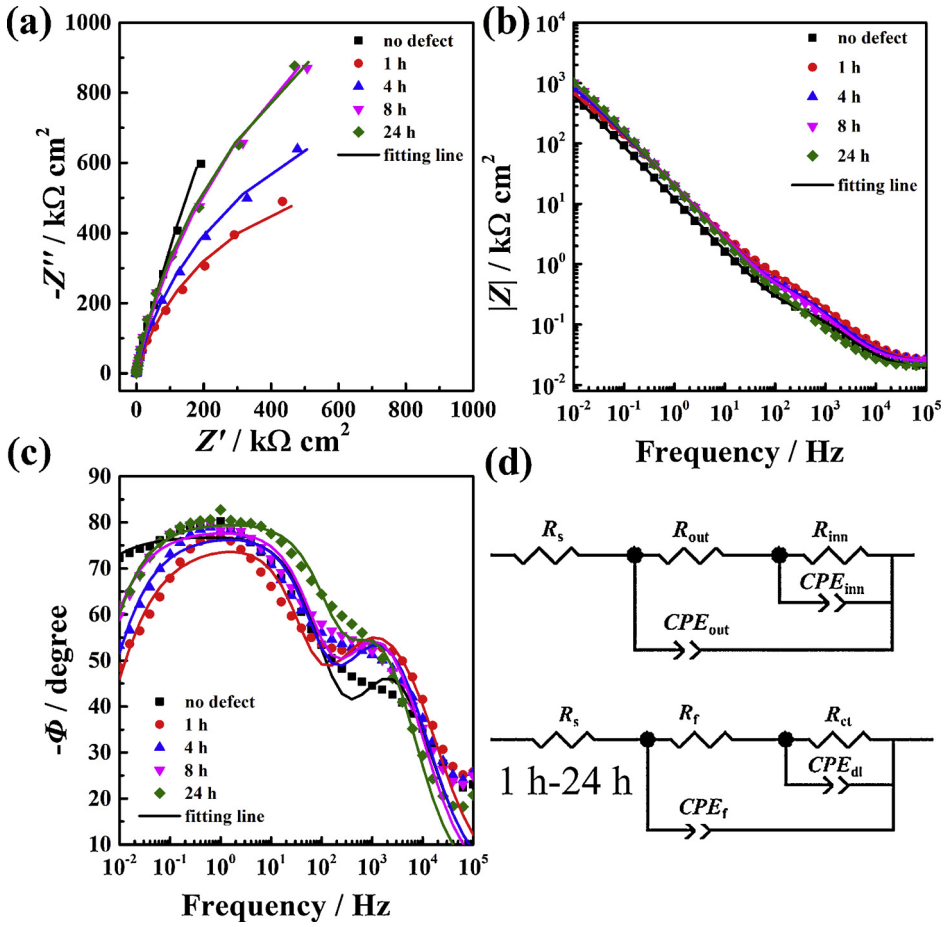

Fig. 10. Nyquist plots, (b) Impedance-frequency Bode plots and (c) Phase-frequency Bode plots of ZnAl-LDH-VOx with an artificial defect in 3.5 wt.% NaCl solution after immersion for different time; (d) The equivalent circuit used to simulate EIS data at different stages.

CPE_f represent the resistance and constant phase element of protective films formed from vanadates. According to the fitting results in Table 5, R_{ct} increased gradually from $3229 \pm 1799\ k\Omega\ cm^2$ to $5461 \pm 2381\ k\Omega\ cm^2$ after immersion for 24 h.

In Fig. 11, the EIS spectra changes of ZnAl-LDH-VOx-La are shown. The impedance arc in the Nyquist spectra of the sample decreased obviously upon the presence of the defect. However, the arc increased significantly after immersion for 8 h. This phenomenon reflects the self-healing ability of ZnAl-LDH-VOx-La. The sample could realize self-reparation when corrosion was initiated. It can be seen clearly from Fig. 11b that the impedance in a wide range of high frequencies was remarkably higher than that of the other samples due to the existence of an insulative air film on the sample surface. This result was in good agreement with the phase angle plot vs. frequency in Fig. 11c, where the black line (intact ZnAl-LDH-VOx-La) shows high phase angle peaks at high frequencies. After the defect was made, the phase angle peak at high frequencies disappeared, indicating the escaping of air film due to the presence of artificial defect. Besides, a new peak in the range of 10^3 to 10^4 Hz appeared probably due to the formation of a film by the combined action of vanadates and laurates. This peak became unclear gradually with time going on maybe mainly due to formation of a denser and more compact reparation film by the vanadates. The first equivalent circuit in Fig. 11d is used to fit EIS data of ZnAl-LDH-VOx-La without defect, which is the same as that in Fig. 9d for fitting ZnAl-LDH-La without defect. In the second circuit in Fig. 11d, the first time constant was related to the reparation film at the defect caused by vanadates and laurates and the second one corresponded to the electrochemical activity. R_{ct} is the charge transfer resistance and CPE_{dl} is the double layer capacitance. In addition, R_f and CPE_f mean the resistance and constant phase element of protective films formed from vanadates and laurates. According to the fitting results in Table 6, the changes of R_{ct} values demonstrated the self-healing ability of the ZnAl-LDH-VOx-La samples.

Table 7 presents the EIS fitting results of ZnAl-LDH-NO_3-, ZnAl-LDH-La, ZnAl-LDH-VOx and ZnAl-LDH-VOx-La without defects after immersion in 3.5 wt.% NaCl solution for 1 h, respectively. According to Table 7, the resistance of the outer LDH layer varied greatly. The R_{out} value of ZnAl-LDH-NO_3- was $25.7 \pm 4.4\ \Omega\ cm^2$, while the intercalation of vanadates led to a value of $147.5 \pm 17.3\ \Omega\ cm^2$. The result may be related to the great affinity of vanadates with the interlayer. As a result, it is difficult for chlorides to get into the gallery of LDH by anion exchange reaction and thus the resistance of the outer LDH layer increased. As for ZnAl-LDH-La and ZnAl-LDH-VOx-La, the outer LDH layer resistance increased to 153525 ± 18335 and $63263 \pm 33720\ \Omega\ cm^2$, respectively. The underlying reason for this phenomenon was that an air film existed on the sample surface and water cannot permeate into the outer loose LDH layer. In addition, the intercalation of laurates and vanadates was also able to increase the difficulties of chloride attack. Therefore, this layer was protected well and the layer resistance increased greatly. The value of R_{inn} can be listed in the following order: ZnAl-LDH-VOx-La > ZnAl-LDH-VOx > ZnAl-LDH-La > ZnAl-LDH-NO_3-. This result demonstrated the better protection ability of ZnAl-LDH-VOx-La than that of ZnAl-LDH-VOx or ZnAl-LDH-La, verifying the synergetic effect of the co-intercalated anions.

Fig. 12 illustrates the evolution of R_{ct} of different samples along with immersion time upon the appearance of artificial defect. As can be seen from Fig. 12, the R_{ct} value was quite small for the sample of ZnAl-

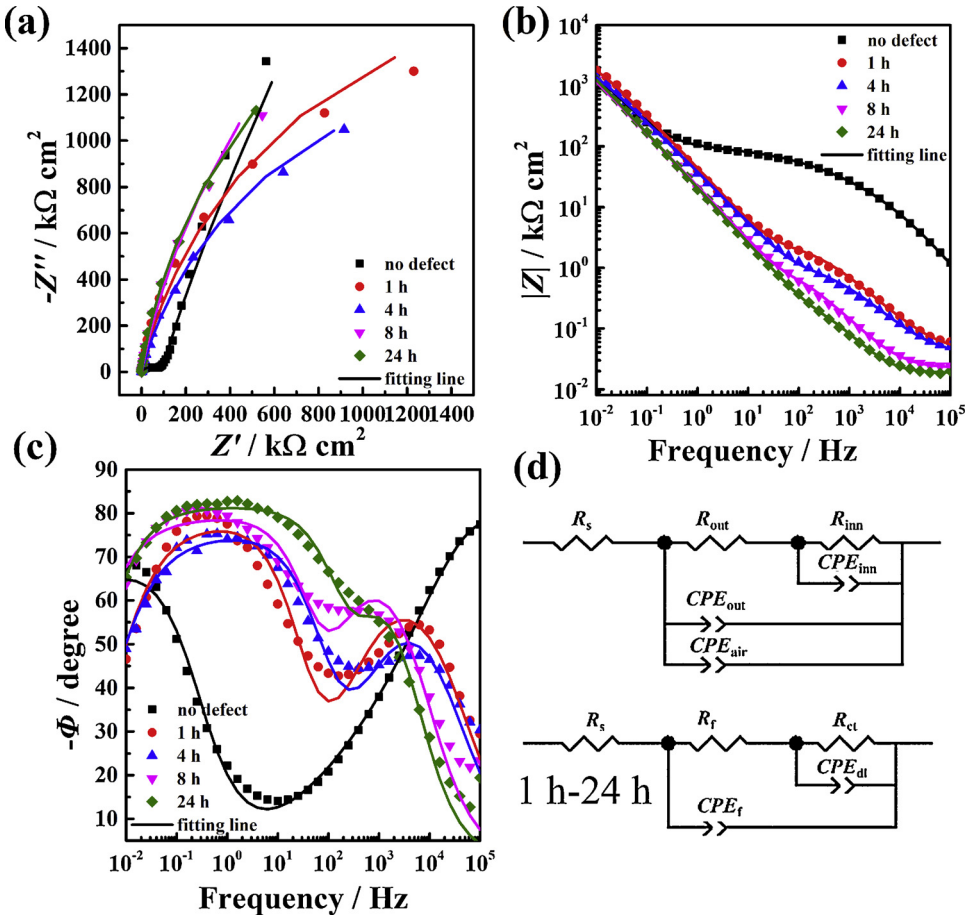

Fig. 11. Nyquist plots, (b) Impedance-frequency Bode plots and (c) Phase-frequency Bode plots of ZnAl-LDH-VOx-La with an artificial defect in 3.5 wt.% NaCl solution after immersion for different time; (d) The equivalent circuit used to simulate EIS data at different stages.

Table 2
The parameters fitted from EIS results in Fig. 7.

Al	R_s (Ω cm^2)	R_{ct} (kΩ cm^2)	*CPE*		R_L (kΩ cm^2)	*L* (H cm^2)
			Y_0(10^{-5} Ω^{-1} cm^{-2} s^n)	*n*		
1 h	23.1 ± 5.0	37.6 ± 12.1	10.1 ± 3.5	0.75	10.6 ± 4.1	31058 ± 16489
8 h	22.5 ± 4.2	28.3 ± 8.3	6.2 ± 1.6	0.77	\	\
24 h	22.9 ± 3.2	30.7 ± 1.4	5.4 ± 1.7	0.80	\	\

Table 3
The parameters fitted from EIS results in Fig. 8.

ZnAl-LDH-NO_3-	R_s (Ω cm^2)	R_{ct} (kΩ cm^2)	CPE_{dl}	
			Y_0 (10^{-6} Ω^{-1} cm^{-2} s^n)	*n*
1 h	22.8 ± 1.8	120.6 ± 17.1	8.8 ± 0.9	0.92
4 h	33.0 ± 12.0	118.0 ± 8.6	8.8 ± 0.9	0.92
8 h	22.6 ± 1.5	121.9 ± 10.0	9.1 ± 0.8	0.92
24 h	23.2 ± 1.5	150.0 ± 9.7	9.6 ± 1.0	0.92

LDH-NO_3-. This can be ascribed to the occurrence of corrosion at the defect site. It increased a little bit along with the immersion time resulting from the accumulation of corrosion products. As for ZnAl-LDH-La, R_{ct} dropped obviously after the defect appeared and then it continued to decrease with time going on, indicating further development of corrosion. It can be concluded that the intercalated laurates cannot provide efficient protection for the underlying substrate even though the R_{ct} values were larger than those of ZnAl-LDH-NO_3-. ZnAl-LDH-VOx and ZnAl-LDH-VOx-La present similar trend. Both the values of R_{ct} increased gradually with the prolonged immersion time and kept almost stable after 24 h. This result clearly demonstrate the self-healing capability of ZnAl-LDH-VOx and ZnAl-LDH-VOx-La. When the defect appeared, corrosion was initiated quickly. The released vanadates interacted with the surface and formed compact films at the defect sites, therefore, corrosion was inhibited in this way.

The EN test was also used to evaluate the difference in corrosion protection ability of different LDH films. Fig. 13 demonstrates the Hilbert spectra of EN current signal obtained for blank Al, ZnAl-LDH-NO_3-, ZnAl-LDH-La, ZnAl-LDH-VOx and ZnAl-LDH-VOx-La with artificial defects after 24 h immersion in 3.5 wt.% NaCl solution. As can be seen from Fig. 13a, large low frequency contribution appeared along the whole time axis for blank Al, ZnAl-LDH-NO_3- and ZnAl-LDH-La, indicating the trend of general corrosion. On the contrary, low frequency components decreased considerably for the sample of ZnAl-LDH-VOx and ZnAl-LDH-VOx-La while obvious signals of high frequency components along the entire time axis occurred. It has been reported that high frequency components show tendency toward localized corrosion at the defect sites [47]. Therefore, it can be concluded

Table 4
The parameters fitted from EIS results in Fig. 9.

ZnAl-LDH-La	R_s (Ω cm^2)	R_f (kΩ cm^2)	CPE_f		R_{ct} (kΩ cm^2)	CPE_{dl}	
			Y_0(10^{-6} Ω^{-1} cm^{-2} s^n)	n		Y_0 (10^{-6} Ω^{-1} cm^{-2} s^n)	n
1 h	61.5 ± 25.7	\	\	\	398.1 ± 0.1	3.5 ± 2.7	0.81
4 h	56.5 ± 8.3	15.4 ± 6.5	1.5 ± 0.5	0.77	408.2 ± 134.0	4.7 ± 1.3	0.78
8 h	44.3 ± 10.5	14.6 ± 4.2	3.2 ± 1.5	0.74	246.9 ± 34.3	3.8 ± 2.6	0.88
24 h	39.1 ± 10.6	1.0 ± 0.4	5.4 ± 0.5	0.72	234.6 ± 67.8	2.8 ± 0.1	0.87

Table 5
The parameters fitted from EIS results in Fig. 10.

ZnAl-LDH-VOx	R_s (Ω cm^2)	R_f (kΩ cm^2)	CPE_f		R_{ct} (kΩ cm^2)	CPE_{dl}	
			Y_0(10^{-6} Ω^{-1} cm^{-2} s^n)	n		Y_0 (10^{-6} Ω^{-1} cm^{-2} s^n)	n
1 h	26.1 ± 3.8	1.0 ± 0.2	5.4 ± 1.6	0.77	3229 ± 1799	6.3 ± 2.5	0.93
4 h	26.7 ± 3.2	0.6 ± 0.1	5.3 ± 0.8	0.81	3695 ± 1745	6.3 ± 2.1	0.94
8 h	26.5 ± 2.5	0.5 ± 0.1	5.1 ± 0.4	0.82	4750 ± 1250	6.3 ± 2.0	0.94
24 h	24.9 ± 4.5	0.3 ± 0.1	5.6 ± 0.8	0.86	5461 ± 2381	6.9 ± 1.4	0.95

Table 6
The parameters fitted from EIS results in Fig. 11.

ZnAl-LDH-VOx-La	R_s (Ω cm^2)	R_f (kΩ cm^2)	CPE_f		R_{ct} (kΩ cm^2)	CPE_{dl}	
			Y_0(10^{-6} Ω^{-1} cm^{-2} s^n)	n		Y_0 (10^{-6} Ω^{-1} cm^{-2} s^n)	n
1 h	38.3 ± 2.8	2.4 ± 0.4	2.0 ± 0.3	0.75	5480 ± 1500	3.3 ± 0.3	0.88
4 h	33.4 ± 3.2	0.8 ± 0.4	2.7 ± 0.2	0.78	4612 ± 1272	3.5 ± 0.3	0.89
8 h	21.7 ± 0.6	0.7 ± 0.4	4.4 ± 0.8	0.85	5783 ± 619	3.6 ± 0.3	0.91
24 h	19.5 ± 0.8	0.3 ± 0.1	4.9 ± 0.6	0.88	5440 ± 870	3.1 ± 0.5	0.93

Table 7
The parameters fitted from EIS results in Figs. 7–11.

Sample	CPE_{air}		R_s (Ω cm^2)	R_{out} (Ω cm^2)	CPE_{out}		R_{inn} (kΩ cm^2)	CPE_{innout}	
	Y_0 (10^{-10} Ω^{-1} cm^{-2} s^n)	n			Y_0 (10^{-6} Ω^{-1} cm^{-2} s^n)	n		Y_0 (10^{-6} Ω^{-1} cm^{-2} s^n)	n
ZnAl-LDH-NO_3-	\	\	17.1 ± 0.2	25.7 ± 4.4	5.8 ± 0.8	0.99	308.3 ± 75.9	13.2 ± 1.4	0.79
ZnAl-LDH-La	10.3 ± 2.7	0.98	22.0 ± 1.9	153525 ± 18335	1.6 ± 0.8	0.41	1319 ± 42	8.7 ± 1.9	0.95
ZnAl-LDH-VOx	\	\	18.9 ± 1.9	147.5 ± 17.3	6.8 ± 0.1	0.80	6466 ± 484	7.7 ± 1.6	0.92
ZnAl-LDH-VOx-La	12.1 ± 1.5	0.99	30.3 ± 9.8	63263 ± 33720	0.6 ± 0.1	0.46	46044 ± 6204	5.1 ± 1.4	0.88

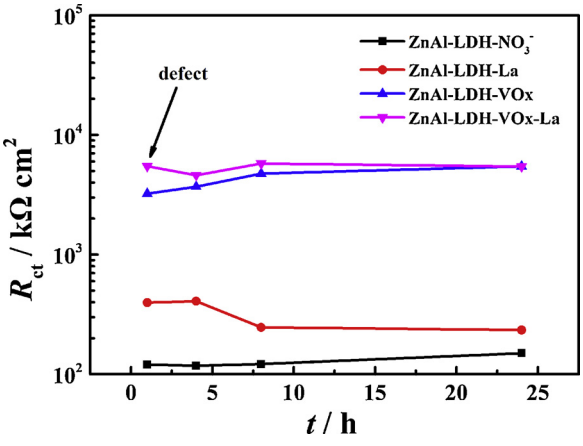

Fig. 12. The evolution of R_{ct} of different samples along with immersion time upon the appearance of artificial defect.

that a protective film was formed at the scratched area, which prevented further corrosion propagation towards general corrosion, on the contrary, restricted the corrosion activity to the local sites [48]. The above result verified the strong self-healing ability of ZnAl-LDH-VOx and ZnAl-LDH-VOx-La, which supported the EIS data in Figs. 7–11 powerfully.

The morphology of the scratched area after immersion in 3.5 wt.% NaCl for 24 h was observed carefully by SEM. As shown in Fig. 14 a1-a2, lots of corrosion products can be observed at the defect of ZnAl-LDH-NO_3-, indicating serious corrosion. The accumulation of the corrosion products were responsible for the slight increase of the R_{ct} values in Table 3. As for the sample of ZnAl-LDH-La (Fig. 14b1–b2), corrosion products can also be observed clearly, however, the amount was slightly smaller than that in the case of ZnAl-LDH-NO_3-, which can be attributed to the protective effect of laurates to some degree. In Fig. 14c1–c2 and d1-d2, almost no corrosion products can be observed in the defect area of ZnAl-LDH-VOx and ZnAl-LDH-VOx-La, suggesting their excellent protection effect for the exposed substrates upon the presence of artificial scratches.

3.2.3. EIS investigations of LDH samples without an artificial defect

The influence of the co-intercalation of vanadates and laurates on the corrosion protection effect of LDH films without artificial defect was also studied by EIS investigations. Different LDH samples were immersed in 3.5 wt.% NaCl for a long time and EIS spectra were collected

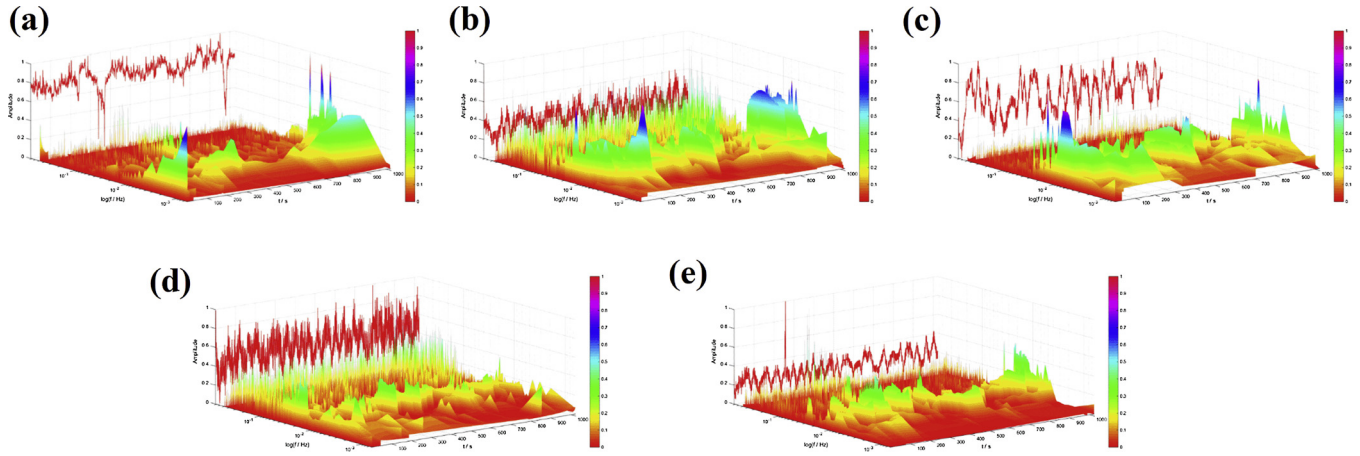

Fig. 13. The Hilbert spectra of EN current signal obtained for (a) blank Al, (b) ZnAl-LDH-NO_3-, (c) ZnAl-LDH-La, (d) ZnAl-LDH-VOx and (e) ZnAl-LDH-VOx-La with an artificial defect after 24 h immersion in 3.5 wt.% NaCl solution.

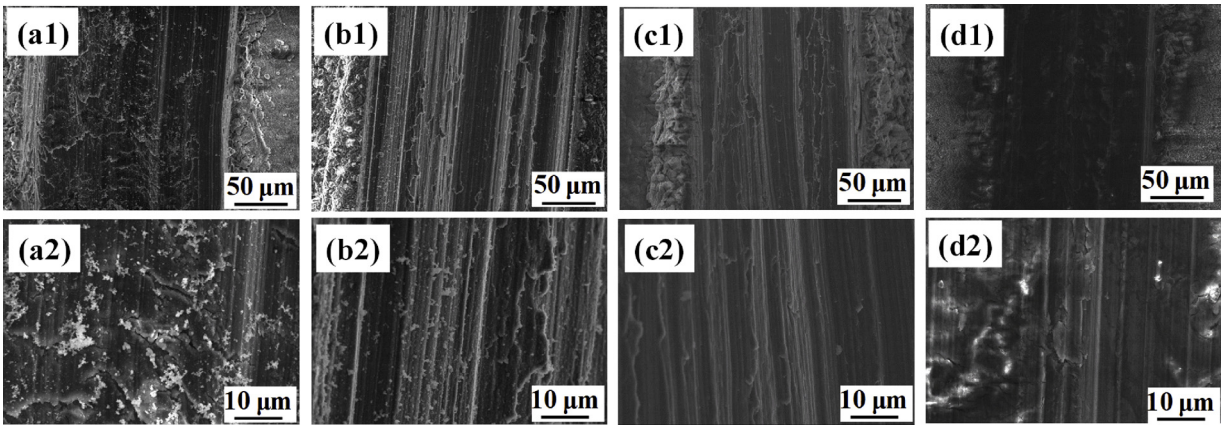

Fig. 14. The morphology of (a1-a2) ZnAl-LDH-NO_3-, (b1-b2) ZnAl-LDH-La, (c1-c2) ZnAl-LDH-VOx and (d1-d2) ZnAl-LDH-VOx-La with an artificial defect after 24 h immersion in 3.5 wt.% NaCl solution.

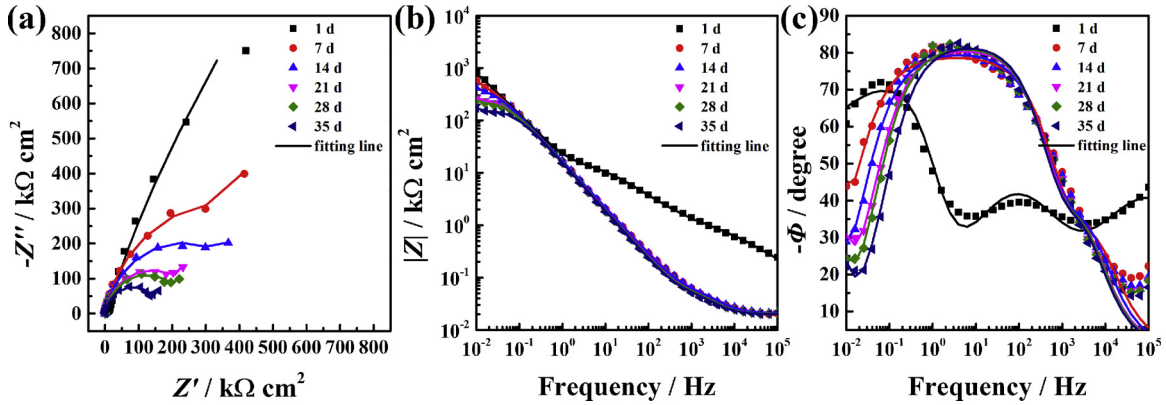

Fig. 15. (a) Nyquist plots, (b) Impedance-frequency Bode plots and (c) Phase-frequency Bode plots of ZnAl-LDH-La without an artificial defect in 3.5 wt.% NaCl solution after immersion for different time.

at certain intervals.

In our previous unpublished work, the long-term corrosion protection mechanism of ZnAl-LDH-NO_3- was investigated by monitoring EIS spectra changes for a long period up to 39 d. The result indicated that the ZnAl-LDH-NO_3- film could provide efficient protection for the Al substrate for 21 d, resulting from the physical barrier role of the inner LDH film itself and the anion exchange reaction between the intercalated nitrates and the chlorides in the solution. After 28 d, the substrate suffered from serious corrosion.

Fig. 15 presents the EIS results of ZnAl-LDH-La in 3.5 wt.% NaCl solution in a period of 35 d. As can be seen from Fig. 15a clearly, the impedance was still higher than that of ZnAl-LDH-NO_3- even though the impedance arc of ZnAl-LDH-La decreased gradually. The main reason is that the air on the superhydrophobic surface escaped and the corrosive medium penetrated into the LDH film. The total resistance of this system can be ascribed to the air film on the superhydrophobic surface and the physical barrier role of the LDH film itself. In addition, the anion exchange reaction between laurates and chlorides was hard to

Table 8
The parameters fitted from EIS results in Fig. 15.

ZnAl-LDH-La	R_s (Ω cm^2)	R_{out} (Ω cm^2)	CPE_{out}		R_{inn}(kΩ cm^2)	CPE_{inn}	
			Y_0 (10^{-6} Ω^{-1} cm^{-2} s^n)	n		Y_0 (10^{-6} Ω^{-1} cm^{-2} s^n)	n
1 d	39.9	1242	1.3	0.61	1420.5	6.9	0.95
7 d	19.9	74.2	4.9	0.89	817.8	6.9	0.89
14 d	20.1	80.9	4.7	0.90	476.6	6.7	0.90
21 d	20.3	72.4	5.1	0.91	286.2	6.9	0.91
28 d	20.5	72.5	4.8	0.92	253.7	6.9	0.92
35 d	20.3	68.5	4.9	0.92	171.1	6.8	0.92

take place probably due to the steric repulsion effect of the long chain of laurates, preventing the attack of chlorides to some extent. The corresponding evidence can be found in Fig. 19. The anion exchange reaction between laurates and chlorides was still incomplete after a long immersion period of 35 d. The first equivalent circuit in Fig. 9d was used to simulate the EIS data and the obtained results were shown in Table 8. As can be seen from Table 8, the value of R_{out} decreased from 1242 to 74 Ω cm^2 after 7 d and kept almost stable until 35 d. This was because the air film escaped and water penetrated into the porous outer LDH layer. The R_{inn} value decreased gradually because corrosion solution ran through the inner LDH layer and reached the interface between the metal substrate and the inner LDH layer. Although corrosion was initiated, the time constant related to the electrochemical activity was not introduced for fitting EIS data because the corresponding parameter cannot be fitted well at a low frequency of 0.01 Hz.

The EIS spectra of ZnAl-LDH-VOx at different time are shown in Fig. 16. The impedance arc declined significantly after immersion for 77 d, suggesting occurrence of serious corrosion. Correspondingly, the phase angle peak narrowed obviously after 77 d. It is remarkable that the resistance of this system was much larger than ZnAl-LDH-NO_3- and ZnAl-LDH-La. The increased corrosion protection ability was mainly due to the released vanadates in addition to the physical barrier role and the anion exchange characteristic of the film. The vanadates act as effective inhibitors in corrosion prevention by forming a protective film at the defect sites. The XRD spectra in Fig. 19 also demonstrated that the anion-exchange reaction was difficult between vanadates and chlorides because some vanadates still existed in the interlayer space after immersion in NaCl solution for 112 d. The underlying reason is that vanadates with high charges have great affinity with the interlayer and cannot be replaced by chlorides easily. The first equivalent circuit in Fig.10d was used to simulate the EIS data and the corresponding fitting results are shown in Table 9. The gradual increase in R_{inn} in an immersion period of 63 d was likely caused by the inhibition effect of vanadates. The dramatic decrease of R_{inn} after immersion for 77 d in Table 9 suggested that corrosion cannot be inhibited anymore and it

Table 9
The parameters fitted from EIS results in Fig. 16.

ZnAl-LDH-VOx	R_s(Ω cm^2)	R_{out} (Ω cm^2)	CPE_{out}		R_{inn} (kΩ cm^2)	CPE_{inn}	
			Y_0(10^{-6} Ω^{-1} cm^{-2} s^n)	n		Y_0 (10^{-6} Ω^{-1} cm^{-2} s^n)	n
1 d	17.0	91.7	9.8	0.85	2147	5.9	0.94
7 d	16.6	87.9	9.5	0.86	1405	5.9	0.94
14 d	18.3	133.2	9.3	0.86	2647	5.7	0.94
21 d	16.8	114.7	9.6	0.85	3234	5.5	0.94
42 d	20.4	202.8	8.2	0.86	4507	5.7	0.93
63 d	21.7	245.9	7.8	0.86	5892	5.5	0.93
70 d	19.5	181.4	8.6	0.86	1750	5.5	0.93
77 d	18.7	181.4	8.4	0.86	222.0	6.9	0.91
91 d	22.4	297.9	8.2	0.85	213.0	6.6	0.91
112 d	18.8	177.9	9.2	0.85	106.7	7.9	0.90

propagated quickly.

Fig. 17 demonstrates the EIS spectra changes of ZnAl-LDH-VOx-La in a long immersion period. It can be seen clearly that the impedance arc kept almost stable during an immersion period of 91 d in spite of some fluctuations. The impedance arc decreased slightly after 112d. The result indicated that ZnAl-LDH-VOx-La was able to provide effective protection for the underlying substrate in a longer time in comparison with ZnAl-LDH-VOx. It can be concluded that the co-intercalation of inhibitors and low surface energy species could play a synergistic role in the protection performance of the film. On one hand, the intercalated vanadates and laurates prevented the attack of chlorides jointly. The evidence can be found in Fig. 19, where the vanadates and laurates still existed in the gallery of LDHs and neither of them were replaced by chlorides completely after a long immersion of 112 d. On the other hand, the vanadate interacted with the surface and a protective film can be formed at the defect site when corrosion was initiated. At present it is not sure whether laurates participated in the formation of this protective film and more evidence is needed in the future. The first equivalent circuit in Fig. 9d was also used to simulate the EIS data of ZnAl-LDH-VOx-La in a long immersion period. As can be seen from Table 10, the value of R_{out} was obviously larger than other samples in the whole immersion period. In addition, R_{inn} increased obviously until 63 d and then decreased after 77 d, however, the values were almost one order larger than that of ZnAl-LDH-VOx after the same immersion time. The result indicated the superior protection effect of the ZnAl-LDH-VOx-La and provided another powerful evidence for the synergetic effect of the co-intercalated anions.

As stated above, the compact inner LDH layer act as the most important physical barrier against the attack of water molecules, therefore, R_{inn} can be regarded as an important parameter for evaluation of film protection ability. Thus, the R_{inn} values at different immersion time

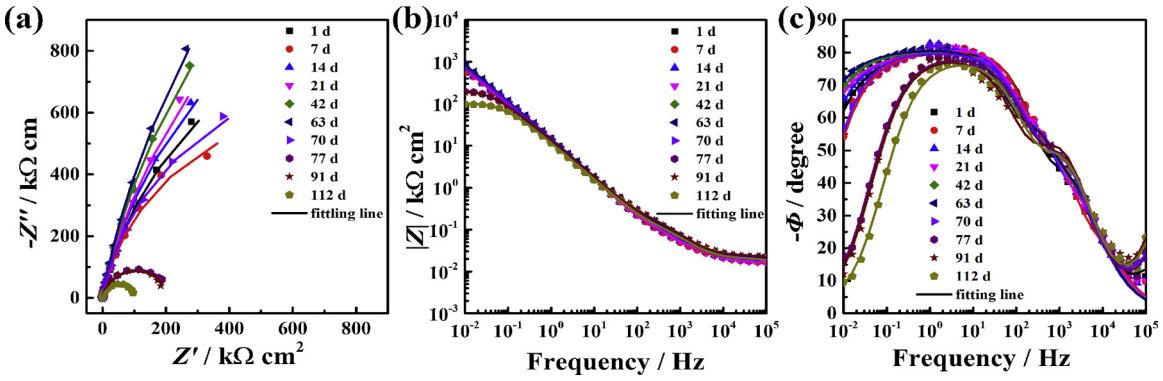

Fig. 16. (a) Nyquist plots, (b) Impedance-frequency Bode plots and (c) Phase-frequency Bode plots of ZnAl-LDH-VOx without an artificial defect in 3.5 wt.% NaCl solution after immersion for different time.

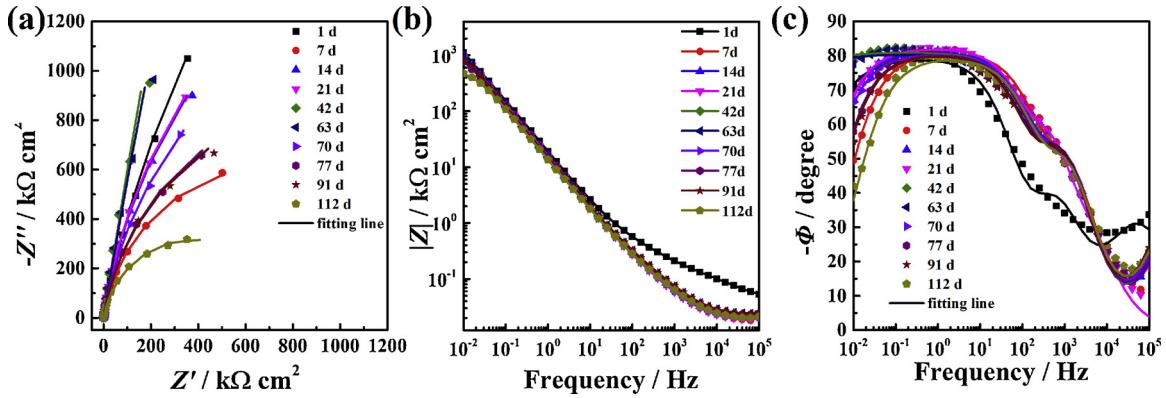

Fig. 17. (a) Nyquist plots, (b) Impedance-frequency Bode plots and (c) Phase-frequency Bode plots of ZnAl-LDH-VOx-La without an artificial defect in 3.5 wt.% NaCl solution after immersion for different time.

Table 10
The parameters fitted from EIS results in Fig. 17.

ZnAl-LDH-VOx-La	R_s (Ω cm^2)	R_{out} (Ω cm^2)	CPE_{out}		R_{inn} (kΩ cm^2)	CPE_{inn}	
			Y_0 (10^{-6} Ω^{-1} cm^{-2} s^n)	n		Y_0 (10^{-6} Ω^{-1} cm^{-2} s^n)	n
1 d	52.3	290.6	2.8	0.79	22190	7.4	0.88
7 d	18.8	165.7	6.7	0.88	1460	5.1	0.92
14 d	21.0	228.2	6.7	0.88	4636	5.2	0.92
21 d	19.5	181.3	6.8	0.89	4503	5.3	0.92
42 d	21.3	218.2	6.8	0.88	30270	6.1	0.91
63 d	24.0	308.2	6.6	0.88	27480	5.8	0.91
70 d	19.9	193.3	7.5	0.87	3484	6.0	0.91
77 d	22.1	235.8	7.1	0.87	2153	5.9	0.91
91 d	24.0	298.0	6.8	0.87	2117	5.8	0.91
112 d	19.7	180.5	7.9	0.86	773.2	6.3	0.90

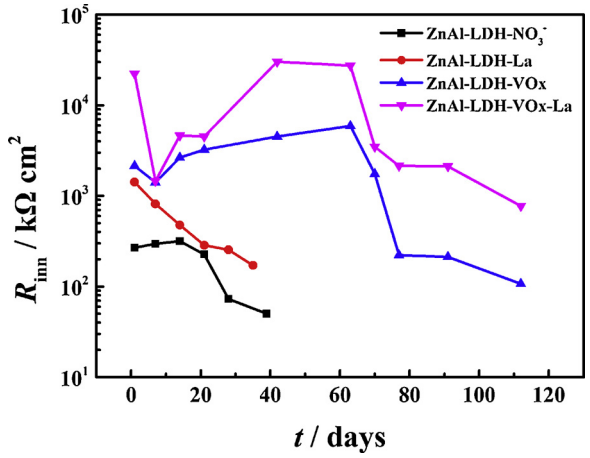

Fig. 18. The evolution of R_{inn} of different samples along with immersion time.

of various samples were plotted, which were shown in Fig. 18. Clearly, ZnAl-LDH-NO_3- and ZnAl-LDH-La presented a declining trend with the immersion time, where the sample with laurates possessed higher R_{inn} values. This result may be related to the hydrophobic air film on the surface and the steric repulsion towards water molecules and chlorides by laurates. For ZnAl-LDH-VOx and ZnAl-LDH-VOx-La, the R_{inn} values were significantly higher than those of ZnAl-LDH -NO_3- and ZnAl-LDH-La in the whole immersion period. Both of them increased continuously until 63 d and then started to decrease, and the values of ZnAl-LDH-VOx-La were significantly higher than those of ZnAl-LDH-VOx.

After a long time of immersion in 3.5 wt.% NaCl solution, different samples were collected and subjected to XRD and EDS characterization.

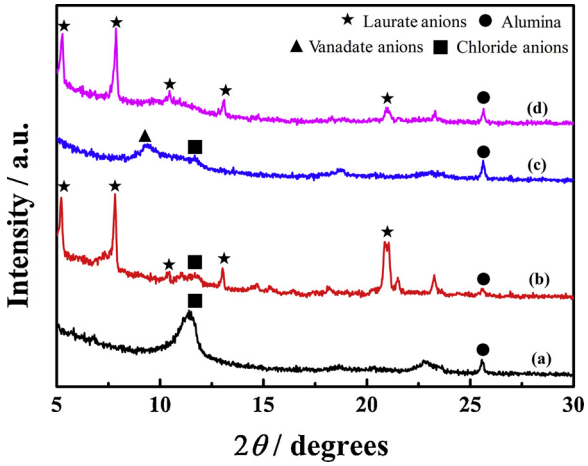

Fig. 19. XRD spectra of samples (a) ZnAl-LDH-NO_3- (39 d), (b) ZnAl-LDH-La (35 d), (c) ZnAl-LDH-VOx (112 d) and (d) ZnAl-LDH-VOx-La (112 d) after immersion in 3.5 wt.% NaCl solution for different time.

The obtained result is presented in Fig. 19 and 20, respectively. It should be noted that all the characteristic peaks attributed to various anion have been identified by different symbols in Fig. 19. It is worthy to note that these results collaborated each other strongly. As can be seen from Fig. 19a, ZnAl-LDH-NO_3- after immersion of 39 d presents typical peaks of (003) and (006) plane of LDH at about 11.7°and 22.8°, which corresponded to the intercalation of chlorides. According to the Bragg's law, the gallery height was calculated to be 0.76 nm. This result indicated that nitrates were replaced by the chlorides almost completely. In Fig. 19b, after immersion of 35 d, ZnAl-LDH-La showed both peaks corresponding to chlorides and laurates, which occurred at about 11.7°and 5.1°, 7.7°, 10.4°, 13.0°, respectively. This result suggested that the anion exchange reaction between laurates and chlorides was not complete and some laurates still remained in the gallery. Fig. 19c demonstrated the XRD spectra of ZnAl-LDH-VOx after immersion in NaCl solution for 112 d, the obtained curve showed peaks at about 9.3°and 11.7°, corresponding to (003) plane of LDH intercalated with vanadates and chlorides, respectively. It is worthy to note that the anion exchange reaction was still not complete during a long immersion time of nearly four months. This was most likely due to the strong interaction between vanadates with high charges and the positive hydroxide layer. This high affinity with the layer of vanadates prevented the attack of chlorides strongly, which benefited the sample greatly. The sample of ZnAl-LDH-VOx-La after immersion for 112 d presented the peak ascribed to laurates and the peak related to vanadates was not observed maybe due to the low resolution of the XRD spectra and more evidence can be found in the EDS results.

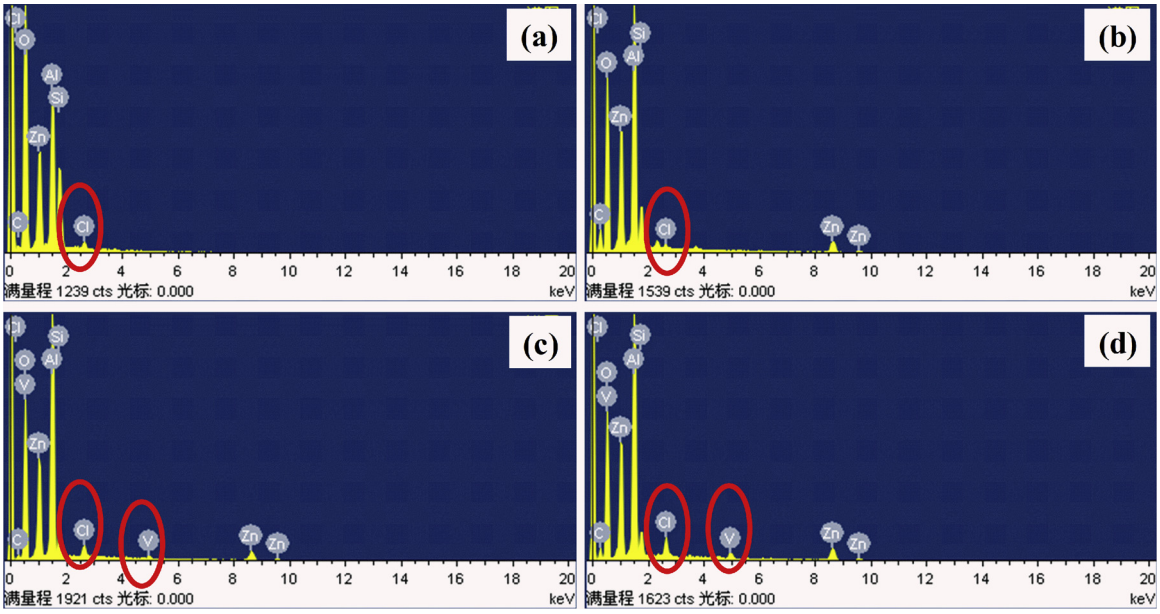

Fig. 20. EDS results of samples (a) ZnAl-LDH-NO_3- (39 d), (b) ZnAl-LDH-La (35 d), (c) ZnAl-LDH-VOx (112 d) and (d) ZnAl-LDH-VOx-La (112 d) after immersion in 3.5 wt.% NaCl solution for different time.

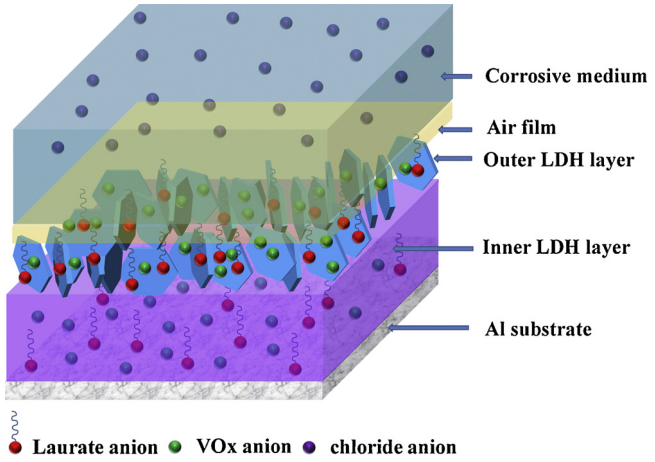

Fig. 21. The schematic illustration of the corrosion mechanism of ZnAl-LDH-VOx-La.

Fig. 20 presents the EDS result of various samples after different immersion period in 3.5 wt.% NaCl solutions. It is clear that the element of Cl appeared in all the EDS spectra, which was in good accordance with the XRD result in Fig. 19 due to the complete or incomplete anion exchange reaction between chlorides and other anions in the gallery of LDH. It should be noted that the element of V was also present in the EDS spectra of ZnAl-LDH-VOx and ZnAl-LDH-VOx-La, verifying that some vanadates still remained in the interlayer space of LDH.

3.2.4. The corrosion mechanism of ZnAl-LDH-VOx-La

Based on the above measurements and discussion, a conceptual illustration to present the corrosion protection mechanism of ZnAl-LDH-VOx-La is proposed in Fig. 21. As can be seen from Fig. 21, the physical barrier consists of three components including the air film on the superhydrophobic surface due to the modification of laurates, the outer LDH layer and the inner compact LDH layer between the underlying Al substrate and the outer LDH layer. Both of these two layers were loaded with vanadates and laurate anions. First of all, the above mentioned three layers contributed to prevention of the attack of the corrosive medium by acting as physical barriers jointly. It should be noted that the superhydrophobicity of ZnAl-LDH-La surface can only be maintained in the initial 24 h after immersion in 3.5 wt.% NaCl solutions according to our previous publications [32]. After 24 h, the attractive air on surface escaped and consequently the superhydrophobic surface became hydrophobic. As a result, the physical barrier effect of the air film decreased significantly. The EIS result also supported this conclusion. According to the EIS result, the phase angle in the high frequencies was as high as -80° after immersion for 1 h while it decreased to about -40° after immersion for 1 d. Secondly, the vanadates with high charges interacted strongly with the hydroxide layer of LDH, therefore, it is hard for the chlorides to participate in the anion exchange reaction with the chlorides. In addition, there are still some laurates remaining in the LDH gallery after a lone immersion time, indicating the difficulties of laurates in anion-exchange reaction with chlorides in the immersion period. According to the EIS fitting results above, it can be seen clearly that the co-intercalation of anions results in the further increase of the resistance of the inner LDH layer, verifying the important role of the difficulties in anion-exchange reaction in corrosion protection effect of the LDH films. However, once the corrosive medium penetrated through the three physical barriers and reached the interface between Al and the LDH layer, corrosion can be initiated immediately. At this time, vanadates released by anion exchange with chlorides could adsorb at the defect, resulting in the formation of a protective film and the inhibition to the further development of corrosion, presenting a significant self-healing effect. In addition, the released laurates are also able to adsorb at the defect and prevent the attack of chlorides and water molecules by the steric repulsion effect of the long chain of laurates. It is worthy to note that the co-intercalation of vanadates and laurates demonstrated synergistic effect in comparison with the sample only loaded with inhibitors according to the higher R_{inn} values. In summary, it can be concluded that the ZnAl-LDH-VOx-La co-intercalated with inhibitors and low surface energy species could provide superior protection for Al substrate by the physical barrier role, the anion-exchange property and the synergistic effect of the co-intercalated species. The co-intercalation of two species render the LDH film with multifunctionality and it is of great significance to improve the corrosion protection performance.

4. Conclusion

ZnAl-LDH-VOx-La co-intercalated with vanadates and laurates was successfully immobilized on Al substrate using a simple hydrothermal and immersion method. The laurates endow the LDHs film with superhydrophobic property and the vanadates act as an effective inhibitor. The intercalation of both of them plays a significant role in improving the resistance against corrosion considerably compared with LDHs loaded with only one of them. The presence of vanadates enables the film with self-healing ability upon artificial defect. In addition, the synergetic effect of these two species contributed to the enhanced long-term protection of the film. This idea sparks the versatility of LDHs structure and its more potential application in the field of corrosion protection.

Conflict of interest

The authors declare no competing conflict of interest.

Data availability

The raw/processed data required to reproduce these findings cannot be shared at this time as the data also forms part of an ongoing study.

Acknowledgements

The authors are grateful for the financial support from State Key Project of Research and Development (2016YFC1100300) and National Natural Science Foundation of China (21773199, 21621091).

References

[1] M. Kopeć, K. Szczepanowicz, G. Mordarski, K. Podgórna, R.P. Socha, P. Nowak, P. Warszyński, T. Hack, Self-healing epoxy coatings loaded with inhibitor-containing polyelectrolyte nanocapsules, Prog. Org. Coat. 84 (2015) 97–106.
[2] F. Maia, A.P. Silva, S. Fernandes, A. Cunha, A. Almeida, J. Tedim, M.L. Zheludkevich, M.G.S. Ferreira, Incorporation of biocides in nanocapsules for protective coatings used in maritime applications, Chem. Eng. J. 270 (2015) 150–157.
[3] F. Maia, K.A. Yasakau, J. Carneiro, S. Kallip, J. Tedim, T. Henriques, A. Cabral, J. Venâncio, M.L. Zheludkevich, M.G.S. Ferreira, Corrosion protection of AA2024 by sol–gel coatings modified with MBT-loaded polyurea microcapsules, Chem. Eng. J. 283 (2016) 1108–1117.
[4] J. Carneiro, J. Tedim, S.C.M. Fernandes, C.S.R. Freire, A.J.D. Silvestre, A. Gandini, M.G.S. Ferreira, M.L. Zheludkevich, Chitosan-based self-healing protective coatings doped with cerium nitrate for corrosion protection of aluminum alloy 2024, Prog. Org. Coat. 75 (2012) 8–13.
[5] E. Shchukina, H.Q. Wang, D.G. Shchukin, Nanocontainer-based self-healing coatings: current progress and future perspectives, Chem. Commun. 55 (2019) 3859–3867.
[6] G. Zhang, L. Wu, A.T. Tang, X.X. Ding, B. Jiang, A. Atrens, F.S. Pan, Smart epoxy coating containing zeolites loaded with Ce on a plasma electrolytic oxidation coating on Mg alloy AZ31 for active corrosion protection, Prog. Org. Coat. 132 (2019) 144–147.
[7] M.L. Zheludkevich, J. Tedim, M.G.S. Ferreira, "Smart" coatings for active corrosion protection based on multi-functional micro and nanocontainers, Electrochim. Acta 82 (2012) 314–323.
[8] M.J. Anjum, J.M. Zhao, V. Zahedi Asl, G. Yasin, W. Wang, S.X. Wei, Z.J. Zhao, W.Q. Khan, In-situ intercalation of 8-hydroxyquinoline in Mg-Al LDH coating to improve the corrosion resistance of AZ31, Corros. Sci. 157 (2019) 1–10.
[9] F. Peng, D.H. Wang, H.L. Cao, X.Y. Liu, Loading 5-fluorouracil into calcined Mg/Al layered double hydroxide on AZ31 via memory effect, Mater. Lett. 213 (2018) 383–386.
[10] K.A. Yasakau, A. Kuznetsova, S. Kallip, M. Starykevich, J. Tedim, M.G.S. Ferreira, M.L. Zheludkevich, A novel bilayer system comprising LDH conversion layer and sol-gel coating for active corrosion protection of AA2024, Corros. Sci. 143 (2018) 299–313.
[11] G. Zhang, L. Wu, A.T. Tang, Y.L. Ma, G.L. Song, D.J. Zheng, B. Jiang, A. Atrens, F.S. Pan, Active corrosion protection by a smart coating based on a MgAl-layered double hydroxide on a cerium-modified plasma electrolytic oxidation coating on Mg alloy AZ31, Corros. Sci. 139 (2018) 370–382.
[12] J.D. Zuo, B. Wu, C.Y. Luo, B.Q. Dong, F. Xing, Preparation of MgAl layered double hydroxides intercalated with nitrite ions and corrosion protection of steel bars in simulated carbonated concrete pore solution, Corros. Sci. 152 (2019) 120–129.
[13] Y.H. Cao, S.G. Dong, D.J. Zheng, J.J. Wang, X.J. Zhang, R.G. Du, G.L. Song, C.J. Lin, Multifunctional inhibition based on layered double hydroxides to comprehensively control corrosion of carbon steel in concrete, Corros. Sci. 126 (2017) 166–179.
[14] E. Alibakhshi, E. Ghasemi, M. Mahdavian, B. Ramezanzadeh, A comparative study on corrosion inhibitive effect of nitrate and phosphate intercalated Zn-Al-layered double hydroxides (LDHs) nanocontainers incorporated into a hybrid silane layer and their effect on cathodic delamination of epoxy topcoat, Corros. Sci. 115 (2017) 159–174.
[15] E. Alibakhshi, E. Ghasemi, M. Mahdavian, B. Ramezanzadeh, S. Farashi, Fabrication and characterization of PO_4^{3-} intercalated Zn-Al-layered double hydroxide nanocontainer, J. Electrochem. Soc. 163 (2016) C495–C505.
[16] Y.J. Mei, J.X. Xu, L.H. Jiang, Q.P. Tan, Enhancing corrosion resistance of epoxy coating on steel reinforcement by aminobenzoate intercalated layered double hydroxides, Prog. Org. Coat. 134 (2019) 288–296.
[17] H.Y. Chen, F.Z. Zhang, S.S. Fu, X. Duan, In situ microstructure control of oriented layered double hydroxide monolayer films with curved hexagonal crystals as superhydrophobic materials, Adv. Mater. 18 (2006) 3089–3093.
[18] J. Tedim, M.L. Zheludkevich, A.C. Bastos, A.N. Salak, A.D. Lisenkov, M.G.S. Ferreira, Influence of preparation conditions of layered double hydroxide conversion films on corrosion protection, Electrochim. Acta 117 (2014) 164–171.
[19] L. Wu, Z.C. Zheng, F.S. Pan, A.T. Tang, G. Zhang, L. Liu, Influence of reaction temperature on the controlled growth of Mg-Al LDH film, Int. J. Electrochem. Soc. 12 (2017) 6352–6364.
[20] T. Zhang, H.Q. Yu, Y.M. Zhou, J. Rong, F.X. Qiu, Y.M. Zhang, In situ fabrication and infrared emissivity properties of oriented LDHs films on Al substrates, RSC Adv. 5 (2015) 82415–82420.
[21] A. Mikhailau, H. Maltanava, S.K. Poznyak, A.N. Salak, M.L. Zheludkevich, K.A. Yasakau, M.G.S. Ferreira, One-step synthesis and growth mechanism of nitrate intercalated ZnAl LDH conversion coatings on zinc, Chem. Commun. 55 (2019) 6878–6881.
[22] Y.B. Wang, Y.S. Zhang, B.T. Zhou, C.M. Li, F. Gao, X.P. Wang, D.Q. Liang, Y.Z. Wei, In-situ observation of the growth behavior of ZnAl layered double hydroxide film using EQCM, Mater. & Design. 180 (2019) 107952.
[23] L. Hao, T.T. Yan, Y.M. Zhang, X.H. Zhao, X.D. Lei, S.L. Xu, F.Z. Zhang, Fabrication and anticorrosion properties of composite films of silica/layered double hydroxide, Surf. Coat. Tech. 326 (2017) 200–206.
[24] Y. Zhang, P.H. Yu, J.P. Wang, Y.D. Li, F. Chen, K. Wei, Y. Zuo, LDHs/graphene film on aluminum alloys for active protection, Appl. Surf. Sci. 433 (2018) 927–933.
[25] L.C. Yan, M. Zhou, X.L. Pang, K.W. Gao, One-step in situ synthesis of reduced graphene Oxide/Zn-Al layered double hydroxide film for enhanced corrosion protection of magnesium alloys, Langmuir 35 (2019) 6312–6320.
[26] J. Tedim, A.C. Bastos, S. Kallip, M.L. Zheludkevich, M.G.S. Ferreira, Corrosion protection of AA2024-T3 by LDH conversion films. Analysis of SVET results, Electrochim. Acta 210 (2016) 215–224.
[27] L.D. Wang, Q.F. Zong, W. Sun, Z.Q. Yang, G.C. Liu, Chemical modification of hydrotalcite coating for enhanced corrosion resistance, Corrosion Sci. 93 (2015) 256–266.
[28] G. Zhang, L. Wu, A.T. Tang, S. Zhang, B. Yuan, Z.C. Zheng, F.S. Pan, A novel approach to fabricate protective layered double hydroxide films on the surface of anodized Mg-Al alloy, Adv. Mater. Interface. 4 (2017) 1700163–1700173.
[29] F.Z. Zhang, L.L. Zhao, H.Y. Chen, S.L. Xu, D.G. Evans, X. Duan, Corrosion resistance of superhydrophobic layered double hydroxide films on aluminum, Angew. Chem. 47 (2008) 2466–2469.
[30] X.D. Lei, L.N. Wang, X.H. Zhao, Z. Chang, M.H. Jiang, D.P. Yan, X.M. Sun, Oriented CuZnAl ternary layered double hydroxide films: in situ hydrothermal growth and anticorrosion properties, Ind. Eng. Chem. Res. 52 (2013) 17934–17940.
[31] L. Wu, J.H. Wu, Z.Y. Zhang, C. Zhang, Y.X. Zhang, A.T. Tang, L.J. Li, G. Zhang, Z.C. Zheng, A. Atrens, F.S. Pan, Corrosion resistance of fatty acid and fluoroalkylsilane-modified hydrophobic Mg-Al LDH films on anodized magnesium alloy, Appl. Surf. Sci. 487 (2019) 569–580.
[32] Y.H. Cao, D.J. Zheng, X.L. Li, J.Y. Lin, C. Wang, S.G. Dong, C.J. Lin, Enhanced corrosion resistance of superhydrophobic layered double hydroxide films with long-term stability on Al substrate, ACS Appl. Mater. Inter. 10 (2018) 15150–15162.
[33] X.X. Guo, S.L. Xu, L.L. Zhao, W. Lu, F.Z. Zhang, D.G. Evans, X. Duan, One-step hydrothermal crystallization of a layered double hydroxide/alumina bilayer film on aluminum and its corrosion resistance properties, Langmuir 25 (2009) 9894–9897.
[34] S.K. Poznyak, J. Tedim, L.M. Rodrigues, A.N. Salak, M.L. Zheludkevich, L.F.P. Dick, M.G.S. Ferreira, Novel inorganic host layered double hydroxides intercalated with guest organic inhibitors for anticorrosion applications, ACS Appl. Mater. Inter. 1 (2009) 2353–2362.
[35] A.N. Salak, J. Tedim, A.I. Kuznetsova, M.L. Zheludkevich, M.G.S. Ferreira, Anion exchange in Zn–Al layered double hydroxides: in situ X-ray diffraction study, Chem. Phys. Lett. 495 (2010) 73–76.
[36] J. Tedim, A. Kuznetsova, A.N. Salak, F. Montemor, D. Snihirova, M. Pilz, M.L. Zheludkevich, M.G.S. Ferreira, Zn–Al layered double hydroxides as chloride nanotraps in active protective coatings, Corros. Sci. 55 (2012) 1–4.
[37] Y. Wang, D. Zhang, Z. Lu, Hydrophobic Mg–Al layered double hydroxide film on aluminum: fabrication and microbiologically influenced corrosion resistance properties, Colloid Surf. A-Physicochem. Eng. Asp. 474 (2015) 44–51.
[38] T.T.X. Hang, T.A. Truc, N.T. Duong, P.G. Vu, T. Hoang, Preparation and characterization of nanocontainers of corrosion inhibitor based on layered double hydroxides, Appl. Clay Sci. 67–68 (2012) 18–25.
[39] M.K. Tang, X.J. Huang, Z. Guo, J.G. Yu, X.W. Li, Q.X. Zhang, Fabrication of robust and stable superhydrophobic surface by a convenient, low-cost and efficient laser marking approach, Colloid Surf. A-Physicochem. Eng. Asp. 484 (2015) 449–456.
[40] X. Zhou, H.Y. Yang, F.H. Wang, Investigation on the inhibition behavior of a pentaerythritol glycoside for carbon steel in 3.5% NaCl saturated $Ca(OH)_2$ solution, Corros. Sci. 54 (2012) 193–200.

[41] R. Wang, S.J. Luo, M. Liu, Y.N. Xue, Electrochemical corrosion performance of Cr and Al alloy steels using a J55 carbon steel as base alloy, Corros. Sci. 85 (2014) 270–279.
[42] P. Wang, D. Zhang, R. Qiu, B.R. Hou, Super-hydrophobic film prepared on zinc as corrosion barrier, Corrosion Sci. 53 (2011) 2080–2086.
[43] N.A. Almobarak, M.M. El-Naggar, R.S. Al-Mufraj, O.A. Al-Zoghbi, Carboxylic acids: pitting corrosion inhibitors for carbon steel in alkaline medium and in the presence of chlorides, Chem. Tech. Fuels Oil. 50 (2014) 170–178.
[44] M. Iannuzzi, G.S. Frankel, Mechanisms of corrosion inhibition of AA2024-T3 by vanadates, Corros. Sci. 49 (2007) 2371–2391.
[45] D. Mata, M. Serdechnova, M. Mohedano, C.L. Mendis, S.V. Lamaka, J. Tedim, T. Hack, S. Nixon, M.L. Zheludkevich, Hierarchically organized Li–Al-LDH nanoflakes: a low-temperature approach to seal porous anodic oxide on aluminum alloys, RSC Adv. 7 (2017) 35357–35367.
[46] M. Serdechnova, M. Mohedano, B. Kuznetsov, C.L. Mendis, M. Starykevich, S. Karpushenkov, J. Tedim, M.G.S. Ferreira, C. Blawert, M.L. Zheludkevich, PEO coatings with active protection based on in-situ formed LDH-nanocontainers, J. Electrochem. Soc. 164 (2016) C36–C45.
[47] E. Alibakhshi, E. Ghasemi, M. Mahdavian, B. Ramezanzadeh, Fabrication and characterization of layered double hydroxide/silane nanocomposite coatings for protection of mild steel, J. Taiwan Inst. Chem. E. 80 (2017) 924–934.
[48] E. Alibakhshi, E. Ghasemi, M. Mahdavian, B. Ramezanzadeh, S. Farashi, Active corrosion protection of Mg-Al-PO_4^3 – LDH nanoparticle in silane primer coated with epoxy on mild steel, J. Taiwan Inst. Chem. E. 75 (2017) 248–262.